Influence of non-adiabatic effects on linear absorption spectra in the condensed phase: Methylene blue

Angus J Dunnett, Duncan Gowland, Christine M Isborn, Alex W. Chin, Tim J Zuehlsdorff

Influence of non-adiabatic effects on linear absorption spectra in the condensed phase: Methylene blue

Angus J. Dunnett,[1] Duncan Gowland,[2] Christine M. Isborn,[3] Alex W. Chin,[1] and Tim J. Zuehlsdorff[4, a)]
[1)] *Sorbonne Université, CNRS, Institut des NanoSciences de Paris, 4 place Jussieu, 75005 Paris, France*
[2)] *Department of Physics, King's College London, London WC2R 2LS, United Kingdom*
[3)] *Chemistry and Chemical Biology, University of California Merced, Merced, CA 95343, USA*
[4)] *Department of Chemistry, Oregon State University, Corvallis, Oregon 97331, USA*

(Dated: 9 November 2021)

Modeling linear absorption spectra of solvated chromophores is highly challenging as contributions are present both from coupling of the electronic states to nuclear vibrations and solute-solvent interactions. In systems where excited states intersect in the Condon region, significant *non-adiabatic* contributions to absorption lineshapes can also be observed. Here, we introduce a robust approach to model linear absorption spectra accounting for both environmental and non-adiabatic effects from first principles. This model parameterizes a linear vibronic coupling (LVC) Hamiltonian directly from energy gap fluctuations calculated along molecular dynamics (MD) trajectories of the chromophore in solution, accounting for both anharmonicity in the potential and direct solute-solvent interactions. The resulting system dynamics described by the LVC Hamiltonian are solved exactly using the thermalized time-evolving density operator with orthogonal polynomials algorithm (T-TEDOPA). The approach is applied to the linear absorption spectrum of methylene blue (MB) in water. We show that the strong shoulder in the experimental spectrum is caused by vibrationally driven population transfer between the bright S_1 and the dark S_2 state. The treatment of the solvent environment is one of many factors which strongly influences the population transfer and lineshape; accurate modeling can only be achieved through the use of explicit quantum mechanical solvation. The efficiency of T-TEDOPA, combined with LVC Hamiltonian parameterizations from MD, leads to an attractive method for describing a large variety of systems in complex environments from first principles.

I. INTRODUCTION

Spectroscopy is a key step in the screening of materials and molecules for technological applications such as photovoltaics, in understanding photochemical reactions, and in the investigation of biological processes.[1,2] In condensed phases, the environment can have a significant influence on the spectral peak position and intensity, causing a change in the electronic and nuclear quantum states of the molecule.[3–5] Modeling the effect of the environment on a molecule in an accurate and computationally affordable way is a persistent challenge.[6,7] Additionally, the accurate and affordable quantum treatment of nuclear dynamics and non-adiabaticity is in constant development.[8–11] The exact calculation of experimental spectra in the condensed phase requires a unification of accurate treatment of the non-adiabatic quantum dynamics with proper inclusion of the effects of the environment.[12]

In many cases, transitions involve bright, energetically well-separated states, justifying the use of the Condon approximation. Similarly, if the chromophore is relatively rigid, the harmonic approximation can be made for the shape of the initial and final state adiabatic Born-Oppenheimer potential energy surfaces (PESs).[13,14] This harmonic Franck-Condon approach has been employed using time-dependent (effective for large multi-mode systems) and time-independent (sum over states, effective for smaller systems) techniques, and can be easily extended to include linear effects of the structure on transition dipole moment (Herzberg-Teller effects).[15–19] When the environment interacts weakly with the ground and excited states, combining Franck-Condon calculations with polarizable continuum models for the solvent environment can yield highly effective environment corrected vibronic lineshapes,[20–22] and for systems with stronger coupling to the environment, some of the authors have presented combined ensemble - Franck-Condon approaches to improve lineshapes calculation.[7,23–25]

However, there are many instances where such a Franck-Condon treatment of the absorption spectrum is insufficient. For example, if there is a region of the PES in which excited states intersect, causing a breakdown of the Born-Oppenheimer approximation, electronic states may mix, leading to non-adiabatic effects such as intensity-borrowing between states.[26,27] For polyatomic systems these crossings are ubiquitous, but the Condon approximation relies on such crossings being far from the initial state equilibrium, representing rare events. If such crossings are close to the region of the potential sampled by the ground state, and thus contribute to the absorption

[a)] Electronic mail: zuehlsdt@oregonstate.edu

spectrum via non-adiabatic effects such as vibrationally driven population transfer, it may become effective to utilize the linear vibronic coupling (LVC) Hamiltonian to describe the system dynamics.[28]

Historically the importance and efficacy of the LVC model in describing spectral lineshapes is well reported.[29] One seminal example is the calculation of the second singlet excitation of pyrazine,[30] and a recent egregious example is the UV spectra of cyclopropane.[31] In the latter case, the authors show extreme intensity borrowing from the optically dark A_2' and A_1' states from the E' state, completely transforming the absorption lineshape. Generally, these studies have focused on small high symmetry molecules in the gas phase, where expensive numerical approaches are both feasible and effective.[32] The previously highlighted examples of pyrazine and cyclopropane were successfully modeled using the multiconfigurational time-dependent Hartree (MCTDH) method, which is often regarded as the gold standard in many-body approaches to non-adiabatic problems.[33] Unfortunately, these methods suffer from the 'curse of dimensionality', meaning inclusion of only a few nuclear and electronic degrees of freedom is feasible, and they generally utilize precalculated potential energy surfaces with high level electronic structure methods.[34] Recently, Santoro and co-workers have parameterized the LVC Hamiltonian for a dense manifold of states for larger molecules using more affordable time-dependent density-functional theory. However, these calculations still limit the number of modes in the system by constructing LVC Hamiltonians in vacuum or relying on polarizable continuum models to represent the environment.[35–37]

There are a number of approaches able to circumvent the exponential scaling of many body states through the use of efficient and compact representations of wave functions, such as multilayer (ML-) MCTDH, matrix product states (MPS), and tensor network states.[38–40] A tensor network-based, many body approach that has been developed to handle complex open quantum systems (OQS) problems is the time-evolving density operator with orthogonal polynomials (TEDOPA) algorithm, based on a mapping that transforms one or more environments into a 1D chain of effective oscillator modes with nearest-neighbour coupling (*vide infra*).[41–43] This geometry unlocks the full power of the MPS/Tensor networks ansatz that perform optimally for 1D systems with locally short-range couplings.[44] Indeed, a recent comparison of ML-MCTDH and MPS methods for 1D dipolar chains found that the MPS approach was both faster and required less computational memory to obtain accurate ground states for this class of models.[45]

TEDOPA is in principle numerically exact, can be combined with machine learning and entanglement renormalization methods, and also gives full access to observable bath dynamics, as recently verified through time-resolved excited-state vibrational spectroscopy in bipentacenes.[40,46] However, until recently, accessing finite temperatures required time-consuming sampling over bath configurations. This limitation was overcome, first with the introduction of the thermofield approach, in which a bath of negative energy modes that act like a source of thermal energy are introduced, and later with the mapping of Tamascelli *et al.* to treat a thermal environment by defining a temperature dependent spectral density, leading to so called T-TEDOPA.[47,48] These advances now allow finite temperature OQS dynamics to be extracted from many-body pure state wave function simulations at 0K - offering substantial advantages over other methods in terms of efficiency.[49] In this article we demonstrate how this new capability allows us to predict optical spectra of real-world molecules in realistic environments that can be directly compared to experiments in solution. In achieving this, we will also show how the Dirac-Frenkel variational principle applied to the TEDOPA state allows us to include long-range couplings that prove to be essential for including the energy gap *correlations* that play a determining role in the excited state dynamics and spectra.

We apply this method to the curious case of the linear absorption spectra of the cationic methylene blue (MB) chromophore in aqueous solution. Both the molecular structure and excitation have been shown to be environmentally sensitive, and there are many open questions about the nature of solvent and aggregation of this molecule and how it influences the spectral lineshape.[50,51] Focusing on the monomeric solution, it shows a singular peak ($\lambda_{\max}$ = 664 nm, 1.86 eV) with a broad, almost square, higher energy shoulder (610 nm, 2.03 eV) at half the absorption maximum intensity.[52] Despite its simple lineshape, previous models for this system appear incomplete. The broad shoulder intensity has been previously both significantly under- and over- estimated depending on the electronic structure, solvent model, and vibronic coupling method of choice.[53] For example, a recent study by de Queiroz *et al.* indicates the S_2 state gains some intensity when examining vertical excitations in explicit solvent, suggesting non-Condon effects. Yet in the same study their computation of the $S_0 \rightarrow S_1$ Franck-Condon spectra *in vacuo* overestimates the shoulder intensity.[54]

Here we expand on previous studies of MB by including explicitly quantum mechanical treatment of the solvent polarization on excitation and nuclear dynamics for vibronic lineshapes. Linear absorption spectra are computed using second and third order truncation of a cumulant expansion of the linear response function constructed from energy gap fluctuations along a molecular dynamics trajectory. We also extend the lineshape calculations to include the strong non-adiabatic effects of higher excited states by solving the LVC problem for three electronic states, finding that the S_2 state of MB plays a large role in determining the excited state dynamics and absorption lineshape. In contrast to previous studies parameterizing LVC Hamiltonians from electronic structure theory we show that LVC model parameters can be obtained directly from correlation functions[55] calculated along generally anharmonic molecular dynamics simulations in ex-

plicit solvent environments, capturing solute-solvent configuration and polarization effects.[56]

This paper is structured as such. First, we present background theory defining the linear vibronic coupling problem in the context of our solvated chromophore, methylene blue. Then we present background on the T-TEDOPA method and the novel derivation of the response function for the T-TEDOPA mapping. Next, we take special care to address the nature of the bath correlations for our solvated chromophore, and how they are addressed in the T-TEDOPA framework and tensor network calculations. The computational method for a) ab initio calculation of various linear vibronic coupling parameters of the chromophore, and b) the tensor network calculation of the T-TEDOPA dynamics are then described. In the results section we provide analysis of our chosen molecule's excitations and dynamics, establishing both the importance of considering the dark S_2 state and the efficacy of our choice of Hamiltonians. We then turn to the question of the importance of including correlation between the excited state dynamics and their influence on the spectral lineshape. From these results we identify the role of the S_1-S_2 energy gap, and so explore the range of this value obtained from electronic structure calculations.

II. THEORY

In this work, we consider a three-level electronic system consisting of an electronic ground state S_0 and two electronic excited states, S_1 and S_2, coupled to nuclear degrees of freedom. The nuclear degrees of freedom are described through the spin-boson model (SBM) or Brownian oscillator model (BOM), which makes the assumption that ground- and excited state PESs are harmonic surfaces with the same curvature that only differ by a displacement of their respective minima.[57,58] The BOM Hamiltonian can then be written as:

$$\hat{H}_{\mathrm{BOM}} = \begin{pmatrix} H_0 & V_{01} & V_{02} \\ V_{10} & H_1 & 0 \\ V_{20} & 0 & H_2 \end{pmatrix}, \tag{1}$$

where $V_{0n} = V_{n0}^{\dagger}$ denotes the transition dipole operator between the electronic ground and n^{th} excited state. We also assume that the Condon approximation is valid, such that the dependence of the transition dipole operator on nuclear degrees of freedom can be ignored and $V_{0n}(\hat{\boldsymbol{q}}) \approx V_{0n}$. The nuclear Hamiltonian of the electronic ground state is denoted $H_0(\hat{\boldsymbol{q}})$, and in the BOM the nuclear Hamiltonians for a system with N vibrational modes can be written as:

$$H_0(\hat{\boldsymbol{p}}, \hat{\boldsymbol{q}}) = \sum_j^N \left(\frac{\hat{p}_j^2}{2} + \frac{1}{2}\omega_j^2 \hat{q}_j^2 \right) \tag{2}$$

$$H_1(\hat{\boldsymbol{p}}, \hat{\boldsymbol{q}}) = \sum_j^N \left(\frac{\hat{p}_j^2}{2} + \frac{1}{2}\omega_j^2 \left(\hat{q}_j - K_j^{\{1\}} \right)^2 \right) + \Delta_{01} \tag{3}$$

$$H_2(\hat{\boldsymbol{p}}, \hat{\boldsymbol{q}}) = \sum_j^N \left(\frac{\hat{p}_j^2}{2} + \frac{1}{2}\omega_j^2 \left(\hat{q}_j - K_j^{\{2\}} \right)^2 \right) + \Delta_{02} \tag{4}$$

where Δ_{01} and Δ_{02} are the adiabatic energy gaps between the ground and first electronic excited state, and ground and second excited state, respectively, and atomic units are used throughout. $\mathbf{K}^{\{1\}}$ denotes the displacement vector of the minimum of the first electronic excited state relative to the electronic ground state, and ω_j is the angular frequency of mode j. For the simple BOM Hamiltonian of a three-level system outlined above, the system-dynamics is completely specified by the two spectral densities of system-bath coupling for the first and second electronic excited state:

$$\mathcal{J}_{01}(\omega) = \frac{\pi}{2} \sum_j^N \omega_j^3 \left(K_j^{\{1\}} \right)^2 \delta(\omega - \omega_j), \tag{5}$$

$$\mathcal{J}_{02}(\omega) = \frac{\pi}{2} \sum_j^N \omega_j^3 \left(K_j^{\{2\}} \right)^2 \delta(\omega - \omega_j). \tag{6}$$

Given that the first and second excited state are completely decoupled, the Condon approximation is assumed, and the nuclear degrees of freedom are described by the BOM Hamiltonian, the linear absorption spectrum $\sigma(\omega)$ can then be evaluated exactly in the cumulant formalism[56,57]

$$\sigma(\omega) \propto \omega \int_{-\infty}^{\infty} \mathrm{d}t\, e^{\mathrm{i}\omega t} \left(\chi_{01}(t) + \chi_{02}(t) \right) \tag{7}$$

with

$$\chi_{01}(t) = |V_{01}|^2 e^{\mathrm{i}\omega_{01}^{\mathrm{av}} t} \exp\left(-g\left[\mathcal{J}_{01}\right](t) \right). \tag{8}$$

Here, $\omega_{01}^{\mathrm{av}} = \langle U_{01} \rangle$ is the ground state thermal average of the energy gap operator $U_{01} = H_1 - H_0$ between the electronic ground- and first excited- states, and $g\left[\mathcal{J}_{01}\right](t)$ is the second-order cumulant lineshape function.[57] Truncation of the cumulant expansion at second order is exact for a system with Gaussian fluctuations of the energy gap, as we have for this BOM Hamiltonian. For the purely linear coupling to nuclear degrees of freedom considered in the BOM, $g(t)$ is completely determined by the spectral density and can be written as[57]

$$g\left[\mathcal{J}\right](t) = \frac{1}{\pi} \int_0^{\infty} d\omega\, \frac{\mathcal{J}(\omega)}{\omega^2} \Big[\coth\left(\frac{\beta\omega}{2}\right) [1 - \cos(\omega t)] - \mathrm{i}[\sin(\omega t) - \omega t] \Big]. \tag{9}$$

For the simple BOM Hamiltonian, Eqns. 8 and 9 yield the exact linear spectrum. However, $\hat{H}_{\mathrm{BOM}}$ neglects a number of important effects on an optical absorption spectrum that are present in realistic systems. Even when retaining a harmonic approximation to the ground and excited state potential energy surfaces, allowing the ground- and excited- state vibrational frequencies to differ introduces non-linear energy gap fluctuations for which the second-order cumulant lineshape is no longer exact.[56] The most general Hamiltonian based on harmonic approximations to the PESs is the Generalized Brownian Oscillator Model (GBOM),[56] which allows for differences between the ground and excited state curvature and mode-mixing effects described by the Duschinsky rotation.[59] The GBOM Hamiltonian can be constructed from ground- and excited- state normal mode analysis and can be solved exactly in the Franck-Condon approach.[16–18] Such Franck-Condon calculations are implemented in a range of standard electronic structure packages. Furthermore, the Condon approximation can be relaxed in this formalism through the inclusion of Herzberg-Teller effects.[16,17] It was recently shown by some of the authors that the nonlinear coupling effects introduced in the GBOM Hamiltonian can also be approximately recovered in the cumulant formalism by including a third-order cumulant correction term.[56]

Both the cumulant approach and the Franck-Condon approach based on the GBOM Hamiltonian can be used to construct the linear absorption spectrum in systems where the individual excited states are separated far enough in energy that they can be treated as fully decoupled. However, if electronic excited states intersect in the Condon region, this intersection leads to strong coupling between the two excited states that is dependent on nuclear coordinates, resulting in a breakdown of the Condon approximation and the intensity-borrowing between electronic excited states that is commonly observed in linear absorption spectra of small organic chromophores.[30,31,35,36]

A simple model Hamiltonian that can describe these dynamics is the linear vibronic coupling (LVC) Hamiltonian. For the purpose of the present work, we only consider linear coupling between the two electronic excited states, such that the LVC Hamiltonian can be written as

$$\hat{H}_{\mathrm{LVC}} = \hat{H}_{\mathrm{BOM}} + \sum_{j}^{N} \begin{pmatrix} 0 & 0 & 0 \\ 0 & 0 & \Lambda_j \hat{q}_j \\ 0 & \Lambda_j \hat{q}_j & 0 \end{pmatrix}, \qquad (10)$$

where the couplings Λ_j to the bath in the off-diagonal elements of the Hamiltonian that mixes the first and the second excited state is then specified by the coupling spectral density

$$\mathcal{J}_{12}(\omega) = \frac{\pi}{2} \sum_{j}^{N} \frac{\Lambda_j^2}{\omega} \delta(\omega - \omega_j). \qquad (11)$$

In contrast to the BOM Hamiltonian, in the LVC model the electronic and nuclear Hamiltonians no longer commute, rendering an analytical description of time-evolution unobtainable. Therefore, more sophisticated methods are required, in this case T-TEDOPA. The details of this description of our system dynamics and the linear response function $\chi(t)$ needed for absorption spectra are contained in Sec. II B).

A. The LVC Hamiltonian in complex condensed-phase environment

For a molecule in the gas phase, the LVC Hamiltonian can be described in terms of $3N$-6 well-defined vibrational modes coupling to the electronic excitations. In the condensed phase, such as for a chromophore in solution or embedded in a protein environment, a large number of bath modes couple to the system, including collective chromophore-environment motion. In this case it becomes convenient to consider the spectral densities introduced in the previous section as continuous functions that can be constructed from equilibrium quantum correlation functions of fluctuation operators.[55] The spectral density $\mathcal{J}_{01}(\omega)$ describing the coupling to the first excited state can then be written as

$$\mathcal{J}_{01}(\omega) = \mathrm{i}\theta(\omega) \int \mathrm{d}t \; e^{\mathrm{i}\omega t} \; \mathrm{Im} \; C_{01}(t), \qquad (12)$$

where $\theta(\omega)$ is the Heaviside step function and the quantum autocorrelation function of the energy gap fluctuation operator is given by

$$C_{01}(t) = \langle \delta U_{01}(\hat{\mathbf{q}}, t) \delta U_{01}(\hat{\mathbf{q}}, 0) \rangle, \qquad (13)$$

and $\delta U_{01} = (H_1 - H_0) - \omega_{01}^{\mathrm{av}} = U_{01} - \omega_{01}^{\mathrm{av}}$.

The exact quantum correlation function $C_{01}(t)$ is, in general, impossible to compute for anything but the most simple model systems. A practical approach for complex condensed phase systems is to approximately reconstruct $C_{01}(t)$ from its classical counterpart using quantum correction factors.[60–62] In this work, we use the harmonic quantum correction factor[61,63] that can be derived by equating the classical correlation function with the Kubo-transformed quantum correlation function possessing the same symmetries as its counterpart.[64,65] This choice yields

$$\mathcal{J}_{01}(\omega) \approx \theta(\omega) \frac{\beta\omega}{2} \int \mathrm{d}t \; e^{\mathrm{i}\omega t} \; C_{01}^{\mathrm{cl}}(t), \qquad (14)$$

where $\beta = 1/k_{\mathrm{B}}T$ and $\theta(\omega)$ is the Heaviside step function.

Eqn. 14 enables the computation of spectral densities in complex condensed phase systems directly by evaluating classical correlation functions of electronic excitation energy fluctuations computed along a molecular-dynamics (MD) trajectory on the ground state potential energy surface. However, computing excitation energies from electronic structure methods such as time-dependent density functional theory (TDDFT) yields

adiabatic electronic states, i.e. states that are electronically decoupled but can change their electronic character along the MD trajectory. Instead, to parameterize the LVC Hamiltonian outlined in the previous section, it is necessary to construct coupled *diabatic* states that do not change character along the trajectory, and thus have constant ground- to excited state transition dipole moments.

As with the choice of quantum correction factor,[61,63] the choice of diabatic states is not unique and several approaches exist to construct quasi-diabatic states from adiabatic states.[66–69] For the present example, we are interested in exploring the effect of the coupling between one bright and one dark state close in energy on the optical absorption spectrum. In this case, an efficient diabatization strategy has been outlined previously by Subotnik and co-workers.[70] Following this approach, we define the transition dipole matrix $\mathbf{D}$ as

$$\mathbf{D} = \begin{pmatrix} V_{01}\cdot V_{01} & V_{01}\cdot V_{02} \\ V_{01}\cdot V_{02} & V_{02}\cdot V_{02} \end{pmatrix} \tag{15}$$

Diagonalizing $\mathbf{D}$ results in two states with maximally different transition dipole moments and oscillator strengths. The eigenvectors of $\mathbf{D}$ can then be used to rotate the diagonal matrix of adiabatic excitation energies into a matrix with two diabatic excitation energies on the diagonal and their electronic coupling as the off-diagonal elements. Performing the diabatization procedure for every snapshot along an MD trajectory, it is then straightforward to construct the classical autocorrelation functions $C_{01}^{\mathrm{cl}}(t)$, $C_{02}^{\mathrm{cl}}(t)$ and $C_{12}^{\mathrm{cl}}(t)$, which, after substitution into Eqn. 14, yields the spectral densities defining the LVC Hamiltonian.

The final parameters needed to define the LVC Hamiltonian are the electronic energy gaps Δ_{01} and Δ_{02}. Assuming a linear coupling to vibrational degrees of freedom, these can be constructed from the classical thermal averages of the energy gap fluctuations, such that $\Delta_{01} = \omega_{01}^{\mathrm{av}} - \lambda_{01}^{\mathrm{R}}$. Here, $\lambda_{01}^{\mathrm{R}}$ is the nuclear reorganization energy of electronic state S_1 that can be computed from the spectral density $\mathcal{J}_{01}(\omega)$ as:

$$\lambda_{01}^{\mathrm{R}} = \frac{1}{\pi}\int_0^\infty \frac{\mathcal{J}_{01}(\omega)}{\omega}\mathrm{d}\omega = \frac{1}{2}\sum_j \omega_j^2 \left(K_j^{\{1\}}\right)^2 \tag{16}$$

Using the above parameters, we can define two distinct measures of the energy gap between S_1 and S_2, which is expected to be a key parameter in this system determining the linear absorption spectrum. First, $\Delta_{12} = \Delta_{02} - \Delta_{01}$, which is the difference between the minima of the diabatic S_1 and S_2 potential energy surfaces, and second, $\omega_{12}^{\mathrm{av}} = \omega_{02}^{\mathrm{av}} - \omega_{01}^{\mathrm{av}}$, the thermal average of the diabatic S_1-S_2 energy gap difference, which represents a measure of the separation of the surfaces in the Condon region.

B. T-TEDOPA & the Response Function

In this section we will briefly describe the T-TEDOPA method and show how it may be employed to calculate the response function. We begin by splitting $\hat{H}_{\mathrm{LVC}}$ into three parts

$$\hat{H}_{\mathrm{LVC}} = H_{\mathrm{S}} + H_{\mathrm{I}} + H_{\mathrm{B}}. \tag{17}$$

H_{S} is a system Hamiltonian governing the electronic states

$$H_{\mathrm{S}} = \sum_{\alpha=1}^{2}(\lambda_{0\alpha}^{\mathrm{R}} + \Delta_{0\alpha})\left|S_\alpha\right\rangle\left\langle S_\alpha\right| + \delta(\left|S_1\right\rangle\left\langle S_2\right| + \mathrm{h.c.}), \tag{18}$$

where h.c. denotes the Hermitian conjugate of the preceding terms and $\lambda_{0\alpha}^{\mathrm{R}}$ denotes the reorganization energies of the S_1 and S_2 baths. We have also included for completeness a coupling δ between S_1 and S_2, although in the case of MB this coupling is extremely small. The Hamiltonian H_{I} is the interaction Hamiltonian which describes the coupling to the nuclear degrees of freedom (DOF). We further decompose this interaction Hamiltonian as follows

$$H_{\mathrm{I}} = H_{\mathrm{I}}^{\mathrm{EL}} + H_{\mathrm{I}}^{\delta}, \tag{19}$$

where the energy level interaction Hamiltonian $H_{\mathrm{I}}^{\mathrm{EL}}$ describes the coupling which causes fluctuations in the S_1 and S_2 energies, and where H_{I}^{δ} is responsible for the fluctuations in the S_1-S_2 coupling matrix element. To begin with, we make the assumption that the three fluctuation motions in the system are uncorrelated, and thus we treat the spectral densities $\mathcal{J}_{01}$, $\mathcal{J}_{02}$ and $\mathcal{J}_{12}$ as pertaining to three independent bosonic baths which we label with $\alpha = 1$, 2 and 3 respectively. We will go on to refine this assumption in section II C. Making the transformation to second quantized creation and annihilation operators, we obtain the following forms for the interaction Hamiltonians

$$H_{\mathrm{I}}^{\mathrm{EL}} = -\frac{1}{\sqrt{2}}\sum_{j,\alpha=1}^{2} K_j^{\{\alpha\}}\omega_j^{\frac{3}{2}}(a_{j\alpha}^\dagger + a_{j\alpha})\left|S_\alpha\right\rangle\left\langle S_\alpha\right|, \tag{20}$$

$$H_{\mathrm{I}}^{\delta} = \sum_j \frac{\Lambda_j}{\sqrt{2\omega_j}}(a_{j3}^\dagger + a_{j3})(\left|S_1\right\rangle\left\langle S_2\right| + \mathrm{h.c.}). \tag{21}$$

Finally, the bath Hamiltonian describing the free motion of the nuclei is given by

$$H_{\mathrm{B}} = \sum_{j,\alpha=1}^{3}\omega_j a_{j\alpha}^\dagger a_{j\alpha}. \tag{22}$$

The initial condition is the of product density matrices

$$\rho(0) = \rho_{\mathrm{S}}\otimes\rho^{\{1\}}\otimes\rho^{\{2\}}\otimes\rho^{\{3\}}, \tag{23}$$

where $\rho^{\{\alpha\}}$ is a thermal equilibrium density matrix for bath α with inverse temperature β_α and $\rho_{\mathrm{S}} = |S_0\rangle\langle S_0|$ is the electronic ground state. These thermal density matrices may appear a major problem since they represent statistical mixtures - implying an averaging over a large number of initial states. However, by applying Tamascelli *et al.*'s T-TEDOPA mapping to each bath, we transform these density matrices into vacuum states $\rho^{\{\alpha\}} \rightarrow |0\rangle_\alpha$ - single pure state wave functions - while the bath spectral density picks up a temperature dependence $J(\omega) \rightarrow J_\beta(\omega)$.[47,48] This new *thermal* spectral density, which encodes the detailed balance of thermal emission and absorption in the mode coupling strengths, is defined on the domain $\omega \in [-\infty, \infty]$ and thus introduces effective *negative* energy modes into the bath. The zero-temperature equilibrium correlation function of this spectrally extended environment is identical to that of the original finite temperature environment, and as the reduced system dynamics defined by $\mathrm{Tr}_{\mathrm{E}}\{\rho(t)\}$ can be shown to be uniquely determined by the bath correlation function, the proxy, extended zero temperature environment can be used to obtain finite temperature results.[47] Moreover, the mapping can also be inverted on the bath modes to provide thermal expectations for the nuclei in the original basis.[48,49]

In general, the optical dipole operator is

$$\hat{V} = V_{01}|S_0\rangle\langle S_1| + V_{02}|S_0\rangle\langle S_2| + \mathrm{h.c.}, \tag{24}$$

and the response function is given by

$$\chi(t) = \langle \hat{V}(t)\hat{V}(0)\rangle_{\rho(0)}. \tag{25}$$

Although the T-TEDOPA mapping preserves the dynamics of the system's reduced density matrix, it is not clear that the same can be said for arbitrary multi-time correlation functions,although some progress has recently been made for the case of third-order response within the thermofield approach.[71] However, in the present case the response function can be shown to depend on a reduced density matrix for the system which has been time-evolved from a particular initial state; therefore, we can correctly employ the mapping. Firstly, we expand the thermal expectation of Eq. 25 and rearrange the contents using the cyclic property of the trace

$$\begin{aligned}\langle \hat{V}(t)\hat{V}(0)\rangle_{\rho(0)} &= \mathrm{Tr}\{e^{\mathrm{i}\hat{H}t}\hat{V}e^{-\mathrm{i}\hat{H}t}\hat{V}\rho(0)\} \\ &= \mathrm{Tr}\{\hat{V}e^{-\mathrm{i}\hat{H}t}\hat{V}\rho(0)e^{\mathrm{i}\hat{H}t}\},\end{aligned} \tag{26}$$

where Tr denotes the trace over all electronic and nuclear coordinates and we have dropped the subscript from $\hat{H}_{\mathrm{LVC}}$. Making use of the Condon approximation, we perform the trace over the nuclear DOF first giving

$$\begin{aligned}\langle \hat{V}(t)\hat{V}(0)\rangle_{\rho(0)} &= \mathrm{Tr}_{\mathrm{S}}\{\hat{V}\mathrm{Tr}_{\mathrm{E}}\{e^{-\mathrm{i}\hat{H}t}\hat{V}\rho(0)e^{\mathrm{i}\hat{H}t}\}\} \\ &= \mathrm{Tr}_{\mathrm{S}}\{\hat{V}\rho'_{\mathrm{R}}(t)\} \\ &= \langle \hat{V}\rangle_{\rho'_R(t)}.\end{aligned} \tag{27}$$

Thus, the response function can be expressed as the expectation value of $\hat{V}$ with respect to the reduced system density matrix $\rho'_{\mathrm{R}}(t)$, which has been evolved from an initial state $\hat{V}\rho(0)$. Unfortunately, $\hat{V}\rho(0)$ does not represent a valid initial state, since it contains only off-diagonal components: $|S_1\rangle\langle S_0|$ and $|S_2\rangle\langle S_0|$; therefore, it is not possible to construct a simulation with $\hat{V}\rho(0)$ as an initial condition. Indeed, because $\hat{V}$ is a Hermitian operator, its expectation cannot equate to that of a multi-time correlation function since the latter may be complex valued. However, using the initial state $\rho'_{\mathrm{S}}(0) = |\psi\rangle\langle\psi|$, where $|\psi\rangle = c(|S_0\rangle + V_{01}|S_1\rangle + V_{02}|S_2\rangle)$ and measuring the *non-Hermitian* operator $\hat{V}' = V_{01}|S_0\rangle\langle S_1| + V_{02}|S_0\rangle\langle S_2|$, we find exactly the same expectation value as we would have found had we measured $\hat{V}$ with the invalid initial condition $\hat{V}\rho(0)$. This is because the system's Hamiltonian does not mix S_1 or S_2 with S_0 and thus the additional terms in ρ'_{S}, such as $|S_1\rangle\langle S_2|$, will be projected out by the measurement of $\hat{V}'$. As ρ'_{S} is a valid initial state, and as nothing prevents us from measuring a non-Hermitian operator, it is now straightforward to construct a simulation for $\chi(t)$.

C. Bath Correlations

In the previous section we made the assumption that the three fluctuation motions, corresponding to the two energy levels and the coupling between them, were completely uncorrelated and could thus be treated as arising from three independent baths. While it is normally justified to assume that there is no correlation between the fluctuations of the coupling and those of the energy levels, the bath motions required for these two kinds of fluctuations being of very different natures, the same is not in general true for the fluctuations of the energy levels between themselves. Indeed, by measuring the cross-correlator of the S_1 and S_2 energy fluctuation operators along the MD trajectory

$$C_{\mathrm{cross}}(t) = \langle \delta U_{01}(\hat{\mathbf{q}}, t)\delta U_{02}(\hat{\mathbf{q}}, 0)\rangle, \tag{28}$$

we find a strong, principally positive, correlation between these two motions for MB. This leads, via Eq. 12, to the cross-correlation spectral density $\mathcal{J}_{\mathrm{cross}}$.

As a means of assessing quantitatively the strength and parity of these correlations, we define the normalized cross-correlation spectral density as $\tilde{\mathcal{J}}_{\mathrm{cross}} = \mathcal{J}_{\mathrm{cross}}/\sqrt{\mathcal{J}_{01}\mathcal{J}_{02}}$. This function takes values in the range $[1, -1]$ and has the following interpretation: if $\tilde{\mathcal{J}}_{\mathrm{cross}} = 1$, we have fully positively correlated modes; the bath induced fluctuations of the S_1 and S_2 energies are perfectly in phase - a raising of the S_1 energy being associated with a simultaneous raising of the S_2 energy (although the amplitudes, which are determined by $\mathcal{J}_{01}$ and $\mathcal{J}_{02}$, need not be the same). Similarly, if $\tilde{\mathcal{J}}_{\mathrm{cross}} = -1$, the fluctuations will be perfectly anti-correlated - a raising of the S_1 energy being associated with a lowering of the

S_2 energy (again the amplitudes need not be identical). Finally, if $\tilde{\mathcal{J}}_{\text{cross}} = 0$, the fluctuations are uncorrelated; i.e., the energy fluctuations behave as two independent sources of Gaussian noise.

The normalized cross-correlation spectral density for MB from our energy gap sampling is plotted in SI Fig. 2. We find that, with a few exceptions, the environmental modes are between 40% and 100% positively correlated (further analysis is presented in SI Sec.IX). In order to include these correlations in the dynamical simulations we must generalize the energy level interaction Hamiltonian H_{I}^{EL} to take the following form:

$$H_{\text{I}}^{\text{EL}} = \sum_k \sum_{\alpha\beta} g_k^{\alpha\beta} \left|S_\alpha\right\rangle \left\langle S_\alpha\right| (a_{\beta k}^\dagger + a_{\beta k}), \tag{29}$$

where now, each harmonic bath couples to both the S_1 and S_2 energies. This interaction Hamiltonian is capable of describing arbitrary correlations between the S_1 and S_2 energy fluctuations. The parameters $g_k^{\alpha\beta}$ are determined so as to reproduce the calculated spectral densities $\mathcal{J}_{01}$, $\mathcal{J}_{02}$ and $\mathcal{J}_{\text{cross}}$. The details of the procedure for obtaining $g_k^{\alpha\beta}$ are contained in SI Sec. III. LVC calculations performed using the exact S_1-S_2 cross-correlation are labeled MDCC (molecular dynamics cross-correlated).

There are two important limiting cases of this Hamiltonian. The first occurs when the off-diagonal coupling coefficients vanish ($g_k^{12} = g_k^{21} = 0$), which corresponds to the uncorrelated limit introduced in section II B. In this case the two excited states are each coupled to their own independent bosonic bath with no communication between them. The second limiting case, which we refer to as the fully positively correlated (FPC) limit, occurs when the two columns of the matrix $g_k^{\alpha\beta}$ are identical; i.e., when $g_k^{12} = g_k^{11}$ and $g_k^{21} = g_k^{22}$. In this case, the coupling matrix $g_k^{\alpha\beta}$ possesses a zero eigenvalue and thus H_{I}^{EL} reduces to a coupling of the collective motion of S_1 and S_2 to a *single, shared* bath (whose creation and annihilation operators are the linear combinations $b_k^{(\dagger)} = \frac{1}{\sqrt{2}}\left(a_{1k}^{(\dagger)} + a_{2k}^{(\dagger)}\right)$). The coupling Hamiltonian for this case takes the form

$$H_{\text{I}}^{\text{EL}} = \sum_k \left(g_k^{11} \left|S_1\right\rangle \left\langle S_1\right| + g_k^{22} \left|S_2\right\rangle \left\langle S_2\right|\right) \left(b_k^\dagger + b_k\right). \tag{30}$$

In the FPC limit the energy fluctuations of the two excited states are induced by the same set of modes and thus have no independent character. We interest ourselves in this FPC limit for two reasons: first, it is interesting to consider, from a theoretical point of view, the effect of correlated energy fluctuations on the absorption spectra and excited state dynamics; second, given that for MB most modes are strongly positively correlated, the FPC limit represents a reasonable approximation which carries with it a significant reduction in computational overhead, because of the need to simulate only one bath. One could also consider the fully negatively correlated limit where the coupling would be to the system operator $g_k^{11} \left|S_1\right\rangle \left\langle S_1\right| - g_k^{22} \left|S_2\right\rangle \left\langle S_2\right|$, however this is nonphysical for MB.

III. COMPUTATIONAL DETAILS

A. Molecular Dynamics and Electronic Structure calculations

To sample the energy gap fluctuations needed to generate the necessary correlation functions and spectral densities of MB in water, four independent trajectories of 8 ps length were generated. The same trajectories as generated for a previous study by some of the authors were used,[72] and the full computational details can be found therein. Here, we summarize the main computational details.

To obtain independent starting points for the four trajectories, force field based molecular dynamics simulations were performed in OpenMM,[73] where water was represented by the TIP3P[74] water model and the MB force field parameters were generated using the QUBEKit package.[75] The system was equilibrated as described in Ref. 72 and a 4 ns production run in the NVT ensemble was performed, where atomic positions and velocities were extracted every 1 ns to yield independent starting points for mixed quantum mechanical/molecular mechanical (QM/MM) simulations.

Using the independent starting points, four 10 ps QM/MM trajectories were generated using the inbuilt QM/MM functionality of the TeraChem package.[76] For dynamics, the chromophore and its counter-ion were treated quantum mechanically with the CAM-B3LYP exchange-correlation functional[77] and 6-31+G* basis set, and all water molecules were described by the TIP3P force field. Calculations were performed in the NVT ensemble using a Langevin thermostat with a collision frequency of 1 ps^{-1} and a time-step of 0.5 fs was used throughout. The first 2 ps of each trajectory were discarded to allow for the system to equilibrate after switching the chromophore Hamiltonian from the force field Hamiltonian to the DFT Hamiltonian in the QM/MM simulation, resulting in 8 ps of usable trajectory for each independent trajectory. From these trajectories, snapshots were extracted every 2 fs for calculating vertical excitation energies, yielding a total of 16,000 snapshots from which the classical correlation functions were constructed.

Adiabatic excitation energies on each snapshot were computed using time-dependent density-functional theory (TDDFT) as implemented in the TeraChem code.[78] To evaluate the influence of different choices of TDDFT functional on the S_1/S_2 coupling, vertical excitation energies were either computed at the CAM-B3LYP/6-31+G* level of theory in the Tamm-Dancoff approximation or at the B3LYP/6-31+G* level of theory using full TDDFT.[77,79] This choice is motivated by the fact that

the relative S_1/S_2 energy is very sensitive to the treatment of long range Hartree-Fock exchange in the density functional, with the CAM-B3LYP functional predicting a larger energy difference between S_1 and S_2 (See SI Sec. V for a discussion of the influence of different density functionals on the calculated excited state energies for MB). We note that the use of the B3LYP functional for computing vertical excitation energies does introduce a mismatch between the Hamiltonian generating the ground state dynamics and the Hamiltonian generating the energy gap fluctuations. Such a mismatch can create artifacts in the computed correlation functions and spectral densities of system-bath coupling, as is commonly observed for spectral densities computed with TDDFT using force-field-based MD trajectories.[80–85] However, the ground state properties of MB predicted by CAM-B3LYP and B3LYP are expected to be similar enough that this mismatch has a relatively minor influence on the computed results. We further validate this choice in SI Sec. VIII, where we compare single trajectory spectral densities of B3LYP ground state dynamics in MM water to the mixed CAM-B3LYP/B3LYP and CAM-B3LYP/CAM-B3LYP spectral densities. The spectral densities are fairly consistent, with a small red shift of frequencies for B3LYP ground state dynamics compared to the CAM-B3LYP dynamics.

To fully capture the influence of dynamic polarization of the environment on the energy gap fluctuations, excitation energies are computed by treating every solvent molecule with a center of mass within 6 Å from any chromophore atom fully quantum mechanically in the TDDFT calculation, with the remaining solvent atoms represented by classical point charges. This treatment leads to QM region sizes of the order of ≈ 400 atoms for the TDDFT calculations. Previous research by some of the authors has shown that for some systems, computed couplings of nuclear vibrations to electronic excited state can be very sensitive to the treatment of polarization effects in the environment, thus making large QM regions necessary.[5] To assess whether the coupling between the S_1 and S_2 excited states in MB shows a similar sensitivity to environmental polarization, we recompute all excitation energies using both the B3LYP and the CAM-B3LYP functional, where only the chromophore is treated quantum mechanically and the full solvent environment is represented by classical point charges (see Fig. 2 for an example of the two QM regions considered in this work).

For all computed data sets, the quasi-diabatic states are computed from the adiabatic energies and transition dipole moments following the approach outlined in Ref. 70. This approach yields diabatic S_1 and S_2 energies, as well as their coupling, for every snapshot. Computing classical autocorrelation functions for the diabatic states and the coupling, we can then parameterize an LVC Hamiltonian that contains the full coupling between the chromophore and its complex environment (See Sec. II A). To avoid numerical issues in the Fourier transforms necessary to compute the relevant spectral densities, a decaying exponential of the form $\exp(-|t|/\tau)$ is applied to all classical correlation functions $C^{\mathrm{cl}}(t)$, where $\tau = 500$ fs. Further details of the formalism and implementation of cumulant lineshape calculations based upon $C^{\mathrm{cl}}(t)$ can be found in recent publications by some of the authors, and are available in the MolSpeckPy package.[86]

B. Tensor Network dynamics

In this section we provide the computational details of the simulations carried out to determine the response function $\chi(t)$. Time-evolution of the density matrix under the LVC Hamiltonian was carried out using the one-site Time-Dependent-Variational-Principle method (1TDVP) on tree and chain Matrix-Product-States (MPS).[40,87,88]

An MPS, or tensor train as they are known within the mathematics community, is a data structure that can be used as an efficient representation of many-body quantum states satisfying the one-dimensional form of the area law. Although an MPS can in principle represent a generic wave-function in any number of dimensions, they are most successfully employed when the system in question possesses a chain-like topology with open boundary conditions. One may also extend the MPS concept to consider systems with a quasi- one-dimensional topology, i.e., a tree structure, using so called tree-MPS, provided that there are no loops.[40] The accuracy of the MPS approximation is controlled by a parameter known as the bond-dimension, with a larger bond-dimension providing a more accurate but more expensive representation. For the simulations used to produce the absorption spectra we present here, a maximum bond-dimension of 20 was found to be sufficient.

By employing the chain mapping,[42] it is possible to transform the Hamiltonians described in sections II B and II C into Hamiltonians with the desired topology. We refer to SI Sec. IV for details on this procedure. The tensor network structures resulting from the chain mapping are shown in Fig. 1 for the uncorrelated and FPC limits introduced in section II C, and also for the general MD cross-correlated (MDCC) case. In the case of uncorrelated S_1-S_2 energy fluctuations, the three harmonic baths are transformed to three chains of harmonic oscillators with nearest-neighbour couplings, each coupled to the central system site, resulting in a loop-free tree topology. On the other hand, in the FPC limit, there are only two baths and so one obtains a chain topology. However, since one of the baths couples to both S_1 and S_2 with different spectral densities, one cannot avoid long-range couplings. For example, if one performs a chain mapping with respect to $\mathcal{J}_{01}$, while S_1 will be coupled to the first site only, S_2 will be coupled to every site along the chain. In practice, these long-range couplings introduce only a modest increase in computational complexity within 1TDVP.[87] Specifically, the bond-dimension of

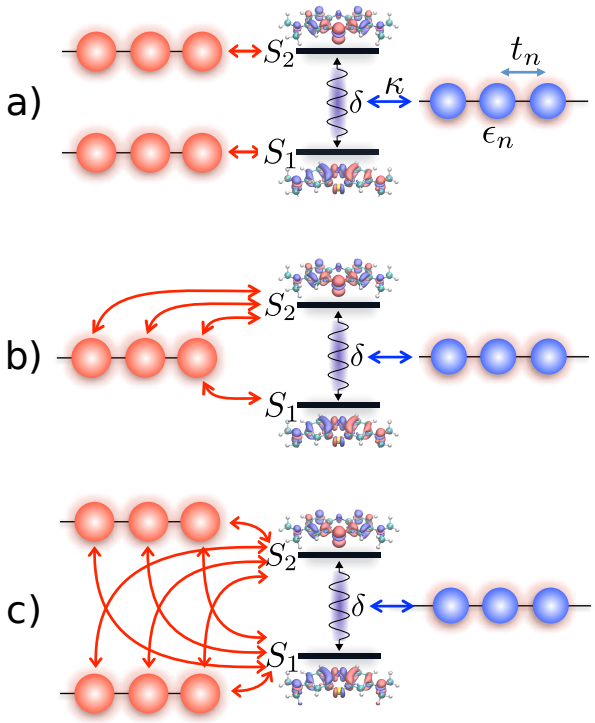

FIG. 1. Tensor network structures used for the various bath configurations considered. (a) Uncorrelated baths, tree-MPS with local interactions only. (b) FPC baths, chain-MPS with some long-range interactions. (c) MDCC baths, tree-MPS with long-range couplings. Bath modes involved in $H_{\rm I}^{\delta}$ (coupling) are shown in blue, while bath modes involved in $H_{\rm I}^{\rm EL}$ are shown in red (tuning). While interactions between the system and the tuning modes may become long-ranged, all intra-chain couplings are nearest-neighbour (t_n) for oscillators of frequency ϵ_n.

the Matrix-Product-Operator (MPO) representation of the Hamiltonian only increases by one. Finally, in the general MDCC case, one again obtains a tree, but now long-range couplings are present on two of the chains.

Two controllable approximations are necessary to make the simulations of these chain mapped Hamiltonians possible. These are: 1) the truncation of the local Fock space of each chain mode to a finite set of states d and 2) the truncation of the semi-infinite chains to a finite number of chain sites N. Both of these approximations introduce errors that are confined by rigorously derived bounds.[89] The linear absorption spectra presented here were found to converge with chain modes truncated to $d = 20$ Fock states and $N = 150$ chain modes for each chain. The observable $\hat{V}'(t)$, used as a proxy for the response function $\chi(t)$, was calculated at 1000 time steps from $t = 0$ up to $t = 240$ fs. The response function was found to decay to a steady state on the time scale of ~ 50 fs, which is physically reasonable for a molecular optical coherence at room temperature. Simulations were performed on nodes consisting of two 12-core Intel Xeon Haswell (E5-2670v3) processors. Approximate simulation times for the uncorrelated, FPC and MDCC limits were, respectively, 9, 8 and 13 hours.

IV. RESULTS

A. Excited States and Spectra Computed Within the Condon Approximation

Before presenting results computed with the LVC Hamiltonian, we first discuss the results of TDDFT excited state calculations and spectra computed within the Condon approximation for the $S_0 \rightarrow S_1$ transition. These results are jointly presented in the calculated absorption lineshapes in Fig. 2 and in SI Sec. V.

For all functionals examined, when excitations are calculated at the S_0, S_1 and S_2 minima, the $S_0 \rightarrow S_1$ transition of MB is bright and the $S_0 \rightarrow S_2$ oscillator strength is consistently low. $S_0 \rightarrow S_2$ shows $\sim$0.5% the intensity of the $S_0 \rightarrow S_1$, indicating that any Franck-Condon approach for modeling $S_0 \rightarrow S_2$ will lead to negligible contributions to the total lineshape. Despite the consistency of the oscillator strengths, the S_1-S_2 vertical energy gap is highly sensitive to functional choice, ranging from 0.06 to 0.67 eV.

Fig. 2 shows the significant difference between the experimental absorption lineshape of MB in water and various Franck-Condon and cumulant lineshape calculations. In all four calculated lineshapes, the shoulder blue shifted 0.15 eV from the 0-0 maxima is underestimated, and the general lineshape significantly underbroadened. For the adiabatic Hessian Franck-Condon (AHFC)[91] calculation, the S_1 excited state geometry and normal modes have been evaluated (at the TDA/CAM-B3LYP/6-31+G* level) and mode mixing effects are accounted for through a Duschinsky rotation.[59] This is equivalent to representing the nuclear degrees of freedom through the generalized Brownian oscillator model (GBOM).[56] The resultant lineshape exhibits two shoulders; one local to the 0-0 peak, and one separated by 0.15 eV and in line with the broad experimental shoulder. As presented in the SI Sec. V B, this AHFC lineshape is reproduced by a range of functionals, for both full TDDFT and TDA, for various solvent models, and when including Herzberg-Teller effects. The main differences between functionals are absolute spectral position (which is pinned to the zero-point corrected energy difference between the ground and S_1 minima), and the presence of the local shoulder. The local shoulder's intensity is correlated with increasing the fraction of long-range exact exchange in the functional. The main shoulder 0.15 eV from the 0-0 transition that is in line with the broad experimental shoulder however is consistently underestimated by all DFT functionals employed here, except by B3LYP with full TDDFT in vacuum, as we

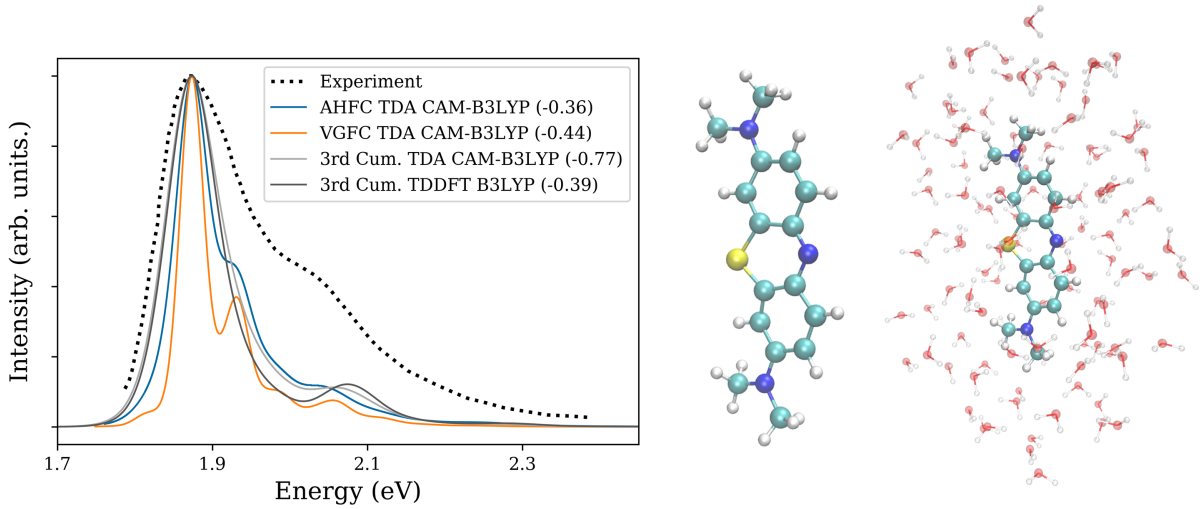

FIG. 2. Methylene blue experimental absorption lineshape and calculated Condon type spectra for the bright S_1 state. Spectra measured in water at low (monomeric) concentration, taken from Ref. 90. Structure of methylene blue (middle), and methylene blue in 6Å water (right) represent the two quantum mechanical environments calculated in this study.

discuss further below.

The other linear absorption lineshapes contained in Fig. 2 are computed in the vertical gradient Franck-Condon (VGFC)[91] and third order cumulant approaches.[56] In the vertical gradient method the underlying vibronic Hamiltonian is the BOM parameterized using the ground state vibrational modes and a single excited state gradient calculation at the ground state minimum. The VG approach thus provides a connection between the AHFC GBOM-type calculations and the effective mapping to the BOM in the cumulant method. The key spectral features are maintained between the AHFC and VGFC methods, indicating that there is only moderate improvement from including Duschinsky rotations or differences between ground and excited state PES curvatures for high frequency modes. However, the VGFC is significantly less broadened, suggesting that changes in frequency and Duschinsky rotation are important for treating low frequency modes. The cumulant lineshapes presented here are calculated in the third order approximation from the diabatized S_1 spectral densities for the system with 6 Å of QM solvent. As will be discussed, the diabatic S_2 dipole intensity along these trajectories are practically zero, leading to no contribution to the total cumulant lineshape. These lineshapes do not display the local shoulder, with the 0-0 peak instead appearing as a broad Lorentzian profile, but do display a secondary vibronic peak in line with the broad experimental shoulder. The thermalization and broadness of the peak appear slightly better modeled by the cumulant than the Franck-Condon approaches, which can be attributed to the extensive sampling which capture low frequency dynamics (including solvent effects) and some contributions from sampling anharmonic regions of the PES.

Although Fig. 2 displays 3rd order cumulant lineshapes, which include corrections due to non-linear couplings to nuclear degrees of freedom that go beyond the simple BOM Hamiltonian, these lineshapes are very similar to the second order cumulant lineshapes (see SI Sec. VII). This similarity shows that non-linear couplings to nuclear degrees of freedom are small, such that the BOM is a good approximation to the underlying dynamics of the system. The appropriateness of the model is echoed by the small skewness values (see SI Sec. VII) for the energy gap fluctuations of both the diabatic S_1 and S_2 surfaces. As the higher order moments of the energy gap fluctuations go to zero, their statistics become exactly Gaussian, then become wholly described by the 2nd order cumulant approximation, and are thus equivalent to a perfect mapping to a set of displaced harmonic oscillators.

In a recent study, de Queiroz *et. al.* performed AHFC calculations of MB in vacuum at the TDDFT/B3LYP/def2-SVP level, which produces a large shoulder in line with experimental results, stemming purely from vibronic contributions to the S_1 state.[54] Our calculations over a range of functionals and lineshape approaches suggest that this large shoulder is anomalous, occurring only for this specific combination of full (non-TDA) TDDFT and B3LYP in vacuum, and could be due to the excited state geometry optimization yielding a state that is of mixed S_1-S_2 character. Many results in their work indicate state mixing. For example, they report difficulties in optimizing excited states, as well as intensity-borrowing effects of the S_2 in snapshot calculations that include explicit solvent. In our studies, this large vibronic shoulder in the lineshape is not reproduced by TDA/B3LYP in vacuum or any methodology in PCM solvent. Similarly, if we perform a vertical gradient Franck-Condon calculation at the TDDFT/B3LYP level in vacuum, the shoulder is removed. We present results for this analysis in SI Sec V C.

In summary, we find that despite considering different approaches to computing the lineshape, a range of density functionals, and the inclusion of environmental effects through the cumulant approach, there is a consistently poor reproduction of the broad experimental spectral shoulder when only considering the transition from the ground state to the bright S_1 state. Furthermore, in static FC calculations, the transition from the ground state to the S_2 state is consistently dark and does not contribute significantly to the lineshape. We also find that the fluctuation statistics of the excited states are closely Gaussian and the BOM is a robust model for the problem at hand. Lastly, TDDFT calculations presented in the SI show that the S_1-S_2 gap is very sensitive to the choice of electronic structure method, and for several functionals the gap is so small that decoupling in the calculation of linear absorption spectra is likely inaccurate. In addition, previous results by de Queiroz *et. al.* show that significant intensity-borrowing between S_1 and S_2 can occur for selected snapshots of MB in explicit solvent,[54] suggesting that both non-adiabatic and solvent effects might play an important role in the experimental lineshape.

We now turn to analysis of the QM/MM ground state ab initio molecular dynamics and the energy gap fluctuations that act as input for constructing the spectral densities that we use to evaluate cumulant spectra and parameterize the LVC dynamics. In Fig. 3 we show a 300 fs window of a single trajectory's energy gaps and corresponding oscillator strengths. On the left of Fig. 3 we show the transition densities when the adiabatic states are well-separated, with the S_1 excitation having a lower energy and high oscillator strength, whilst the S_2 is higher in energy and has low oscillator strength. There are dips in the oscillator strength of the S_1 state at 3076 and 3120 fs which coincide with peaks in the S_2 intensity. As can be seen in the oscillator strengths at around 3200 fs, there are also crossings between the S_1 and S_2 states; the bright and dark states energetically reorder. On the right of Fig. 3, we show transition densities of adiabatic electronic excited states at a point of degeneracy. These represent the S_1 and S_2 states becoming 'left' and 'right' mirrored degenerate excitations. The increase in S_2 dipole intensity for certain regions of the potential energy surface is consistent with the results of de Queiroz *et. al.* seen for individual MD snapshot calculations in explicit solvent.[54] Strong state mixing (as measured by adiabatic S_2:S_1 oscillator strength ratio of 1:3 or greater) occurs for approximately 3.3 % of snapshots at the CAM-B3LYP/TDA/6Å QM solvent level. Thus, non-adiabatic mixing of excited states occurs semi-frequently around the ground state equilibrium. However, this value is significantly enhanced to 16.8% for the B3LYP/TDDFT/6Å QM data set, and would likely further increase when accounting for nuclear quantum effects within the MD sampling of the ground state PES.[24]

Application of the diabatization scheme outlined in Ref. 70 to adiabatic snapshot data is very successful in separating the adiabatic S_1 and S_2 into a bright diabatic S_1 and a dark diabatic S_2 state. These diabatic states are indicated by the dashed lines in Fig. 3. The consistency of these states restores the Condon approximation, at the price of introducing an explicit coupling between the diabatic S_1 and S_2 states that has to be accounted for by solving the LVC Hamiltonian. Applying the quantum correction factor and Fourier transform of the classical correlation functions of diabatic energy gap fluctuations leads to the spectral densities for the ground to S_1, ground to S_2, and coupling spectral densities shown in Fig. 4. $\mathcal{J}_{01}(\omega)$ and $\mathcal{J}_{02}(\omega)$ detail the ground state vibrational frequencies that couple to the electronic states, whilst $\mathcal{J}_{12}(\omega)$ describes the ground state vibrational frequencies that couple the excited states. These peaks can be assigned approximately to vibrational normal modes calculated for the isolated molecule, which we detail in the SI Sec. IX. To summarize, the diabatic S_1 and S_2 are shown to couple to A_1 symmetric modes, whilst the diabatic coupling is driven by asymmetric B_2 modes. Significant contributions to the spectral density range from 110 to 1710 cm^{-1}, with the most intense coupling occurring between the S_2 and the mode at 1710 cm^{-1}, which is a C-C symmetric ring stretching mode.

Diabatic S_1 and S_2 spectral densities and their diabatic coupling spectral density are presented in SI Sec. I, along with the exhaustive table of parameters for the LVC Hamiltonian. The key result of this data is that the average transition dipole moments are quite consistent between electronic structure methods, with the S_2 remaining consistently dark for both CAM-B3LYP and B3LYP in both QM and MM solvent. Similarly, the solvent reorganization energy obtained by integrating the spectral densities (eq. 16) is consistent, and there is minimal change in spectral densities when different functionals are used for the ground state ab initio molecular dynamics. However, the energy gap between the minima of the diabatic potential energy surfaces Δ_{12} is quite sensitive to the functional and environment. This is seen in Δ_{12} having a value of 0.087 eV for CAM-B3LYP in QM solvent, and -0.026 eV in B3LYP MM solvent. This energy gap strongly influences the amount of mixing that occurs between the states in the LVC dynamics.

B. Bath correlation

In Fig. 5 we present calculated lineshapes (left) and excited state population dynamics (right) from T-TEDOPA applied to the LVC Hamiltonian parameterized using the spectral densities and parameters from the CAM-B3LYP data set in 6 Å explicit QM solvent, examining different approaches to treating the bath correlation. To first test the T-TEDOPA method without coupling, we compare the T-TEDOPA approach applied to the LVC Hamiltonian with deactivated S_1-S_2 coupling to the third-order cumulant lineshape. Both these methods have the same pure diabatic spectral densities; however, for the uncou-

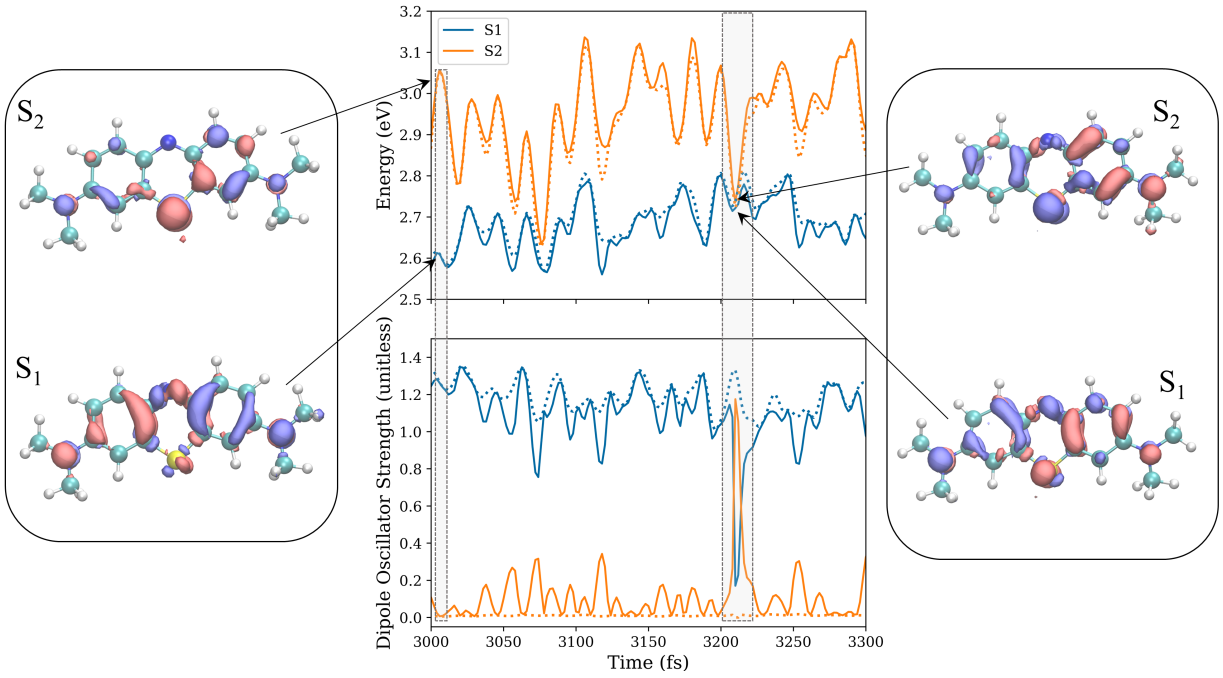

FIG. 3. Excitation energies and oscillator strengths for a segment of trajectory 1 as computed with CAM-B3LYP and a 6 Å QM region. Adiabatic energies and oscillator strengths are shown as solid lines, corresponding diabatic values are shown as dotted lines. The transition densities of the adiabatic S_1 and S_2 states for two specific snapshots along the MD trajectory are also shown.

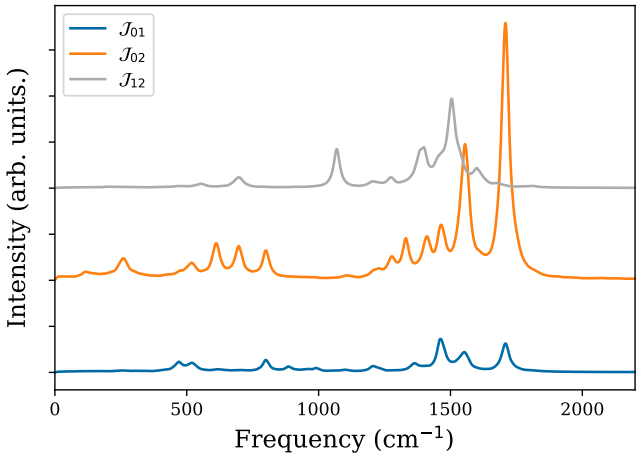

FIG. 4. Spectral densities of the diabatic S_1 and S_2 states, as well as the S_1/S_2 coupling spectral density as computed for the CAM-B3LYP data set in 6 Å explicit QM solvent.

pled LVC approach the total lineshape is given by the sum of the S_1 and the low intensity S_2 contribution, which slightly increases and smooths the high energy shoulder, whereas the third order cumulant approach includes some effects due to non-linear energy gap fluctuations. As expected, the peak maxima are effectively identical (seen in the legend shift values), the onsets are very similar, and they both significantly underestimate the experimental shoulder.

As discussed in the methodology and graphically illustrated in Fig. 1, we utilize three different regimes for describing the nature of the couplings between S_1 and S_2 in the LVC Hamiltonian. The computationally cheapest is the uncorrelated (labeled UC) bath, where the tree-MPS has only local interactions and the cross-correlation between the electronic state fluctuations is assumed to be zero. In the other extreme, the fully positively correlated (FPC) limit, the cross-correlation between fluctuations is unity, such that fluctuations in S_1 drives an equivalent change in S_2 and *vice versa*. There is a bath shared by the states, leading to a chain-MPS with some long-range interactions, and an increase in computational expense over the UC system. Lastly, the more expensive and physical approach is to include the exact structure of the normalized cross-correlation between electronic states. Examining the short-time (first 50 fs) regime of the population dynamics, which strongly influences the linear absorption spectrum, we note significantly different amounts of fast population transfer to S_2 depending on the coupling model. If the states are uncoupled, the S_1 population stays pure. However, allowing any kind of S_1-S_2 coupling leads to a fast (<20 fs) and significant (∼15%) population transfer from S_1 to S_2. This population transfer decreases the main peak intensity in the linear absorption spectrum and increases the intensity of the shoulder. The first 8 fs are very similar between models, indicating a fast transition of a portion of the wavepacket from the S_1 to the S_2 PES via the CI close to the Condon region. The populations quickly differ after this point; for

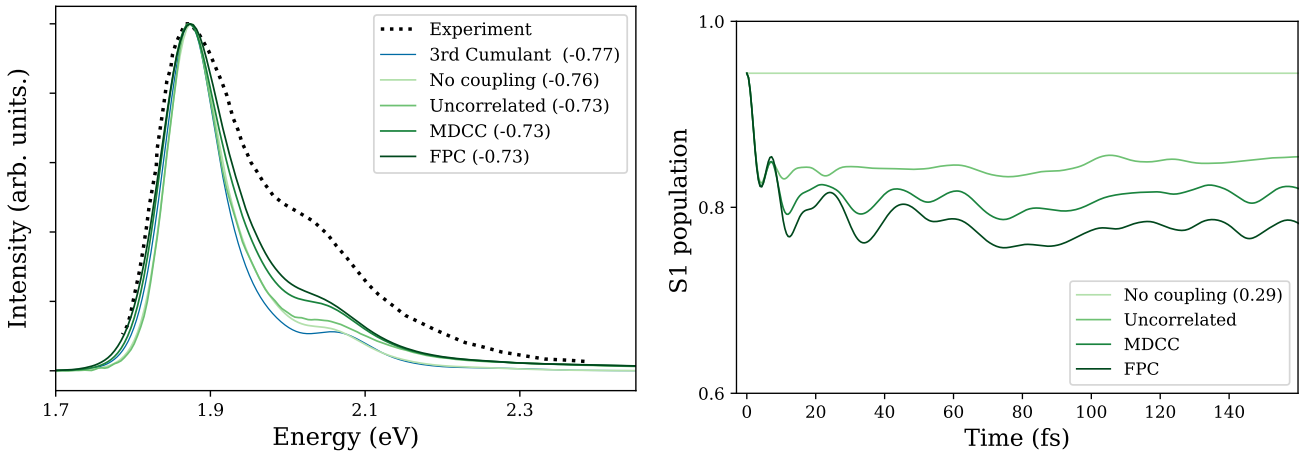

FIG. 5. Effect of tensor network bath configurations on lineshape (left) and S_1 population (right) using the 6Å QM water TDA/CAM-B3LYP/6-31+G* data. Correlated vibrations (up to fully positively correlated - FPC) between S_1 and S_2 drive fast non-adiabatic transitions to the dark S_2 state and increase the broad shoulder intensity. Lineshapes have been shifted by the left legend value to match experiment. Legend value on the right is the average S_1-S_2 gap ω_{12}^{av} in eV.

the UC system the population dynamics evolves into a steady state and further mixing with S_2 is limited, whilst the correlations in the FPC bath persist and drive further population transfer to and from the S_2 state. This population of S_2 is reflected in the absorption lineshapes, with the FPC model displaying a stronger shoulder feature, moving closer to experiment, whereas the change in shoulder intensity for the UC bath is moderate. Lowering the main peak intensity through population transfer also decreases the sharpness of the absorption onset, and FPC most closely matches the experimental onset.

The dynamics and lineshape using the MDCC bath closely mirror FPC, which is rationalized by the fact that the average MD sampled cross-correlation value is 0.8. The key differences in the dynamics of these two models are that the secondary dip is not driven as low as in the FPC dynamics, and the following peak structure is slightly dampened. This dampening could be due to the small cross-correlation value of specific modes or from general lowering of cross-correlation across the entire frequency range. The lower population transfer for the MDCC manifests in the section of the lineshape between the main S_1 and S_2 features and the intensity of the high energy shoulder feature is preserved by the MDCC method.

Therefore, we find that if cross-correlation between states has an average value close to one, the FPC model is a good approximation to the MDCC dynamics and can lead to appropriate lineshapes for the LVC Hamiltonian with reduced computational cost. However, in this case the inclusion of the exact structure of the fluctuations (in MDCC) between electronic states comes with only a modest increase in computational cost due to the efficiency of MPS/T-TEDOPA. Overall, including non-adiabatic transitions appears essential, as significant fast population transfer occurs even when ignoring correlation between the electronic states.

C. Influence of the S_1-S_2 gap

1. Functionals and environment

Having found the spectral shoulder intensity to be strongly sensitive to the population transfer between the electronic excited states, we next consider the parameters in our LVC Hamiltonian. Noting the consistency of the spectral densities, diabatic dipole moments, and reorganization energies between different solvent models and electronic structure methods, the adiabatic energy gap Δ_{12} between the two excited state surfaces presents itself as the most important parameter for this problem.

The computed absolute vertical excitation energies of S_1 and S_2 vary by 0.6 eV depending on the density functional used (see SI Sec. V). We also find that the diabatic S_2 state shows a larger variance in energy depending on the amount of exact exchange in the functional due to having greater charge-transfer character than S_1. This leads to a strong functional sensitivity in the S_1-S_2 gap. In principle, it would be desirable to determine an accurate S_1-S_2 energy gap using higher-level electronic structure methods. However, both the size of the MB molecule and the fact that explicit solvent environment plays a significant role in the value of the energy gap makes precise evaluation prohibitive. Instead, we proceed by calculating the MDCC MPS/T-TEDOPA dynamics and lineshape for parameters calculated in different solvent environments (QM vs MM) and for B3LYP/TDDFT vs CAM-B3LYP/TDA to examine the influence of the LVC parameter choice on the computed lineshape. Fig. 6 summarizes these results, with the legend of the population dynamics (right) indicating the average energy gap

for the given LVC parameterization. The average energy gap ω_{12}^{av} is the energy difference between diabatic S_1 and S_2 averaged over our molecular dynamics configuration sampling around the ground state equilibrium ($\omega_{12}^{\text{av}} = \omega_{02}^{\text{av}} - \omega_{01}^{\text{av}}$), and is a robust measure of the gap between states in the Condon region.

The most extreme average energy gap ω_{12}^{av} values are CAM-B3LYP QM (0.29 eV) and B3LYP MM (0.12 eV). Here, using point charge models for solvent reduces ω_{12}^{av} by 0.05 eV. These values directly translate into the population dynamics; we find that large ω_{12}^{av} leads to a retention of population in S_1, whereas the smallest value leads to the greatest population transfer. For the first 20 fs the population transfer is almost four times larger for B3LYP MM over CAM-B3LYP QM, which directly manifests in the absorption lineshape. Although the trend in population transfer is gap sensitive, the structure and oscillations are remarkably consistent when using MDCC. This consistency stems from the similarity in spectral densities and cross-correlation between data sets.

Also in this figure we present the MDCC and UC populations and lineshape for the CAM-B3LYP/QM data but with the average energy gap artificially reduced by 40%., to match the B3LYP/QM system. For the reduced gap MDCC, the structure of the dynamics is conserved but the population transfer is greater. The short time dynamics are equivalent to B3LYP/QM, but at longer times we see that reducing the gap leads to greater population transfer, with S_2 becoming the majority populated state. However, reducing the energy gap alone is insufficient for increasing the lineshape shoulder. If the bath correlation is ignored (UC) then the dynamics (particularly oscillations) are dampened, and whilst the general population transfer is large, the shoulder is weaker and decays slowly. This finding indicates that the reproducing the shoulder in the lineshape is only possible with an exact description of $\mathcal{J}_{\text{cross}}$ as well as accurate evaluation of the solvent polarized electronic energies.

2. Controlling the average energy gap

Given that our calculations show a large variance in average energy gap and that no singular *ab initio* method presents itself as unequivocally better for the calculation of excited states, we examine how population dynamics and lineshapes change for a range of average gap values. Using the CAM-B3LYP/TDA/6Å QM data set we present in Fig. 7 these results for increments of 20% average energy gap reduction. This range spans an average energy gap value from 0.29 eV to 0.06 eV. This small value is equivalent to the S_1-S_2 vertical excitation energy gap as calculated with TDA/B3LYP/PCM, which is presented in SI Sec. V.

Reducing the gap and utilizing the MDCC model is highly effective at progressing the calculated lineshape towards the broad experimental shoulder, with the best result occurring for the energy gap reduced by 60%. All population dynamics have similar structure, but the driven population transfer to the S_2 state grows increasingly large as the gap closes. This population transfer mostly occurs in the first 25 fs. The intermediate time dynamics (100-150fs) show very similar plateaus in population transfer. The long time oscillations are strongly dampened for gap reduction $> 40\%$.

We conclude that fast $S_1 \rightarrow S_2$ population transfer is the main driver of the broad linear absorption spectral shoulder of the MB monomer in water. However, even with inclusion of non-adiabatic effects using the exact solution to the LVC Hamiltonian and the explicit solvent environment, we are unable to completely recreate the experimental spectra. This discrepancy can be related to several factors. The most practical of these considerations is that although reducing the energy gap in an *a posteriori* manner improves the lineshape, it does not correctly account for changes in the structure of the cross-correlation. Clearly the structure of the cross-correlation is important in driving fast dynamics and spectral shoulder intensity, and even moderate changes can reduce low frequency broadening and more strongly couple high frequency vibrations. Better electronic structure methodologies may lead to more accurate properties, in particular the coupling spectral density and the cross-correlation. Another source of improvement may be the inclusion of non-linear terms beyond our LVC model. For example, although the energy gap fluctuations of the diabatic S_1 and S_2 states seem well described by a linear coupling model given the small corrections the third-order cumulant lineshape provides over the second-order cumulant approach, we are unable to determine how accurately the coupling between S_1 and S_2 is modeled by the LVC Hamiltonian for this system.

V. CONCLUSION

We have presented a novel methodology for the calculation of the LVC Hamiltonian using a tensor network based approach for quantum dynamics and parameterized using data from *ab initio* molecular dynamics and TDDFT. This method has been applied to the large and curious shoulder in the linear absorption spectra of aqueous methylene blue (MB), demonstrating the role of vibrationally driven population transfer from the bright S_1 to the dark S_2.

This methodology is highly attractive as it may be applied to arbitrarily large chromophores in complex environments; capturing the influence of solvent polarization and dynamics, and some anharmonicity, in the spectral densities, whilst still giving exact quantum dynamics. Indeed, the MPS/T-TEDOPA method presents itself as exceptionally computationally efficient and affordable for the evaluation of non-adiabatic dynamics between two electronic states with exact inclusion of cross-correlation by introducing an additional bath. It is readily extendable to a greater number of states, and is particularly ap-

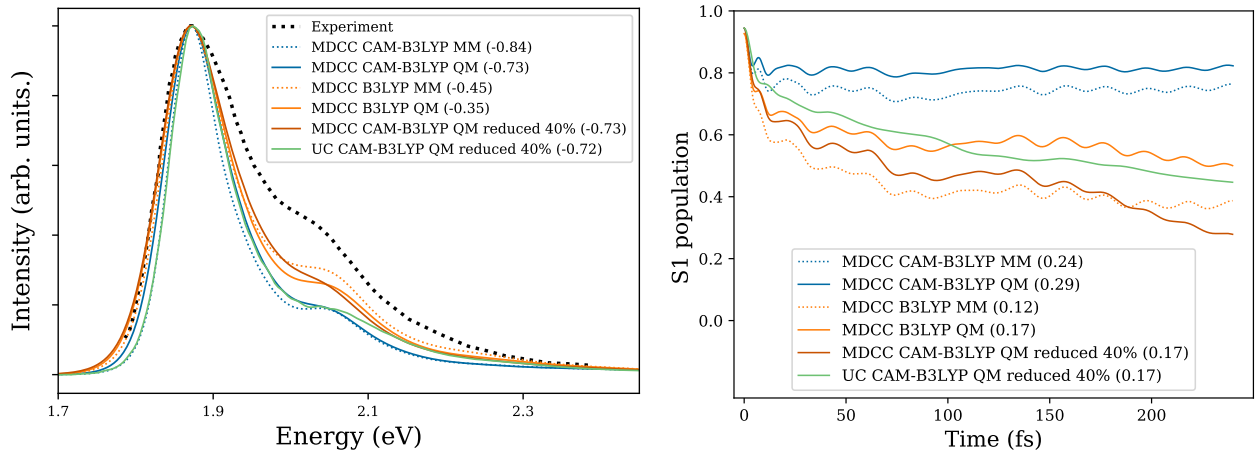

FIG. 6. Using molecular dynamics cross-correlation (MDCC) for bath correlation ($\tilde{\mathcal{J}}_{\text{cross}}$), different functionals and solvent models strongly influence the energy gap between electronic states. This can dramatically increase fast non-adiabatic transitions from the S_1 state and increase shoulder intensity. Lineshapes have been shifted by the left legend value to match experiment in eV. Legend values on the right are the average gap ω_{12}^{av} in eV.

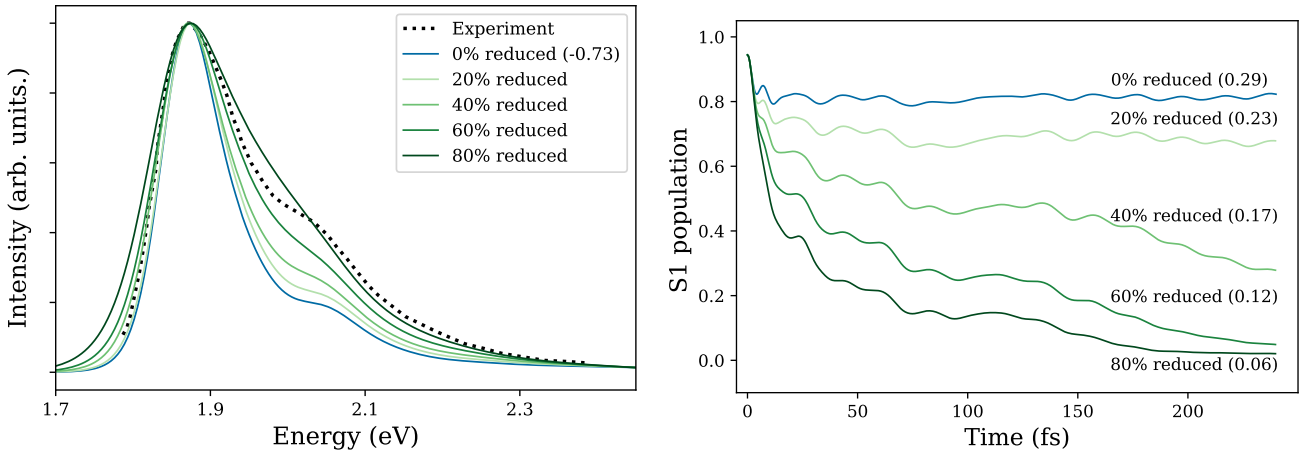

FIG. 7. Using molecular dynamics cross-correlation (MDCC) for bath correlation ($\tilde{\mathcal{J}}_{\text{cross}}$), the reduced average S_1-S_2 gap may be set to a reduced value. For the 6Å QM water TDA/CAM-B3LYP/6-31+G* spectral densities, reducing this value significantly increases the population transfer to the dark S_2 state and increases the absorption shoulder intensity. Lineshapes have been shifted by the left legend value (eV) to match experiment. Legend values on the right are the average gap ω_{12}^{av} in eV.

pealing for complex linear absorption lineshapes, where only short time propagation is required to compute converged spectra. Further investigation of T-TEDOPA, particularly pertaining to the nature of many-time correlation functions and the retention of bath dynamics, is highly promising for the calculation of quantum dynamics and their interpretation in spectroscopy. Some recent studies have made use of bath observables,[40,46] and this is to be examined in the case of MB.

We note several key results for MB. Firstly, the mapping to the BOM, and the extension to the LVC is effective, as measured by the fluctuation statistics. The S_1 and S_2 both couple to high and low frequency modes with A_1 symmetry, whilst the diabatic coupling is due to B_2 modes. Upon calculating the LVC dynamics and lineshape we find it essential to accurately account for both; the correlations between fluctuations in S_1 and S_2, and the average energy gap. The structure of the correlations lead to more effective mixing and show richer oscillatory population dynamics, and the energy gap significantly influences the general population transfer. Most spectral densities and parameters for the LVC are fairly insensitive to the solvent model or the parameters of the TDDFT calculation, with the exception of the average S_1-S_2 gap which is very sensitive and difficult to appraise accurately. Choosing a reasonable value for this parameter when calculating the LVC lineshapes leads to significantly better agreement with experiment. Intriguingly, the excited state population dynamics show signs of a transition in the dominant character of S_1, as the aver-

age energy gap between the bright S_1 and dark S_2 - at the ground state geometry - is reduced. While unimportant at room temperature for the absorption spectrum, the emission spectrum will be highly sensitive to the detailed, non-adiabatic dynamics of the excited states, as they relax in solvent. The present numerically exact methodology can be extended to these problems, and will be pursued in future work.

ACKNOWLEDGMENTS

Calculations were performed using the MERCED computational resource, supported by the National Science Foundation Major Research Instrumentation program (ACI-1429783), as well as the LLNL Pascal supercomputer. A.J.D. acknowledges support from Ecole Doctorale Physique en Ile-de-France (EDPIF ED564). A.W.C. acknowledges support from ANR project No. 195608/ACCEPT. T. J. Z. acknowledges startup funding provided by Oregon State University. C.M.I. was supported by the U.S. Department of Energy, Office of Science, Basic Energy Sciences under Award Number DE-SC0020203.

VI. DATA AVAILABILITY

The data that support the findings of this study are available from the corresponding author upon reasonable request. The cumulant spectra reported in this work were computed with the MolSpeckPy package available at https://github.com/tjz21/Spectroscopy_python_code. All tensor network simulations were performed using the MPSDynamics.jl package available at https://github.com/angusdunnett/MPSDynamics.

[1]F. A. Zucca, J. Segura-Aguilar, E. Ferrari, P. Muñoz, I. Paris, D. Sulzer, T. Sarna, L. Casella, and L. Zecca, "Interactions of iron, dopamine and neuromelanin pathways in brain aging and Parkinson's disease," Progress in Neurobiology **155**, 96–119 (2017).

[2]M. Rivera-Torrente, L. D. Mandemaker, M. Filez, G. Delen, B. Seoane, F. Meirer, and B. M. Weckhuysen, "Spectroscopy, microscopy, diffraction and scattering of archetypal MOFs: Formation, metal sites in catalysis and thin films," Chemical Society Reviews **49**, 6694–6732 (2020).

[3]A. Marini, A. Muñoz-Losa, A. Biancardi, and B. Mennucci, "What is solvatochromism?" Journal of Physical Chemistry B **114**, 17128–17135 (2010).

[4]M. R. Provorse, T. Peev, C. Xiong, and C. M. Isborn, "Convergence of excitation energies in mixed quantum and classical solvent: Comparison of continuum and point charge models," J. Phys. Chem. B **120**, 12148–12159 (2016).

[5]T. J. Zuehlsdorff, H. Hong, L. Shi, and C. M. Isborn, "Influence of Electronic Polarization on the Spectral Density," J. Phys. Chem. B **124**, 531–543 (2020).

[6]C. Puzzarini, J. Bloino, N. Tasinato, and V. Barone, "Accuracy and Interpretability: The Devil and the Holy Grail. New Routes across Old Boundaries in Computational Spectroscopy," Chemical Reviews **119**, 8131–8191 (2019).

[7]T. J. Zuehlsdorff, S. V. Shedge, S.-Y. Lu, H. Hong, V. P. Aguirre, L. Shi, and C. M. Isborn, "Vibronic and environmental effects in simulations of optical spectroscopy," Annual Review of Physical Chemistry **72**, 165–188 (2021), pMID: 33395546, https://doi.org/10.1146/annurev-physchem-090419-051350.

[8]C. Zener, "Non-adiabatic crossing of energy levels," Proc. Roy. Soc. A **33**, 696–702 (1932).

[9]H. D. Meyer and W. H. Miller, "A classical analog for electronic degrees of freedom in nonadiabatic collision processes," The Journal of Chemical Physics **70**, 3214–3223 (1979).

[10]M. Baer, "Introduction to the theory of electronic non-adiabatic coupling terms in molecular systems," *Physics Reports*, **358**, 75–142 (2002).

[11]B. F. E. Curchod and T. J. Martínez, "Ab initio nonadiabatic quantum molecular dynamics," Chem. Rev. **118**, 3305–3336 (2018).

[12]I. Tavernelli, B. F. Curchod, and U. Rothlisberger, "Nonadiabatic molecular dynamics with solvent effects: A LR-TDDFT QM/MM study of ruthenium (II) tris (bipyridine) in water," Chemical Physics **391**, 101–109 (2011).

[13]A. Charaf-Eddin, A. Planchat, B. Mennucci, C. Adamo, and D. Jacquemin, "Choosing a functional for computing absorption and fluorescence band shapes with TD-DFT," Journal of Chemical Theory and Computation **9**, 2749–2760 (2013).

[14]E. Stendardo, F. Avila Ferrer, F. Santoro, and R. Improta, "The absorption and emission spectra in solution of oligothiophene-based push–pull biomarkers: a PCM/TD-DFT vibronic study," Theoretical Chemistry Accounts **135**, 1–17 (2016).

[15]E. V. Doktorov, I. A. Malkin, and V. I. Man'ko, "Dynamical symmetry of vibronic transitions in polyatomic molecules and the Franck-Condon principle," Journal of Molecular Spectroscopy **56**, 1–20 (1975).

[16]F. Santoro, A. Lami, R. Improta, J. Bloino, and V. Barone, "Effective method for the computation of optical spectra of large molecules at finite temperature including the duschinsky and herzberg-teller effect: The qx band of porphyrin as a case study," J. Chem. Phys. **128**, 224311 (2008).

[17]A. Baiardi, J. Bloino, and V. Barone, "General time dependent approach to vibronic spectroscopy including franck–condon, herzberg–teller, and duschinky effects," J. Chem. Theory Comput. **9**, 4097–4115 (2013).

[18]B. de Souza, F. Neese, and R. Izsák, "On the theoretical prediction of fluorescence rates from first principles using the path integral approach," J. Chem. Phys. **148**, 034104 (2018).

[19]R. Berger, C. Fischer, and M. Klessinger, "Calculation of the vibronic fine structure in electronic spectra at higher temperatures. 1. Benzene and pyrazine," Journal of Physical Chemistry A **102**, 7157–7167 (1998).

[20]F. J. A. Ferrer, R. Improta, F. Santoro, and B. V., "Computing the inhomogeneous broadening of electronic transitions in solution: A first-principle quantum mechanical approach," Phys. Chem. Chem. Phys. **13**, 17007–17012 (2011).

[21]F. J. Avila Ferrer, J. Cerezo, J. Soto, R. Improta, and F. Santoro, "First-principle computation of absorption and fluorescence spectra in solution accounting for vibronic structure, temperature effects and solvent inhomogenous broadening," Computational and Theoretical Chemistry **1040-1041**, 328–337 (2014), excited states: From isolated molecules to complex environments.

[22]J. Cerezo, F. J. Avila Ferrer, and F. Santoro, "Disentangling vibronic and solvent broadening effects in the absorption spectra of coumarin derivatives for dye sensitized solar cells," Phys. Chem. Chem. Phys. **17**, 11401–11411 (2015).

[23]T. J. Zuehlsdorff and C. M. Isborn, "Combining the ensemble and Franck-Condon approaches for calculating spectral shapes of molecules in solution," J. Chem. Phys. **148**, 024110 (2018).

[24]T. J. Zuehlsdorff, J. A. Napoli, J. M. Milanese, T. E. Markland, and C. M. Isborn, "Unraveling electronic absorption spectra using nuclear quantum effects: Photoactive yellow protein and green fluorescent protein chromophores in water," J. Chem. Phys. **149**, 024107 (2018).

[25]S. V. Shedge, T. J. Zuehlsdorff, A. Khanna, S. Conley, and C. M. Isborn, "Explicit environmental and vibronic effects in simulations of linear and nonlinear optical spectroscopy," The Journal of Chemical Physics **154**, 084116 (2021), https://doi.org/10.1063/5.0038196.

[26]W. Domcke and D. R. Yarkony, "Role of conical intersections in molecular spectroscopy and photoinduced chemical dynamics," Annual Review of Physical Chemistry **63**, 325–352 (2012).

[27]G. Orlandi and W. Siebrand, "Theory of vibronic intensity borrowing. Comparison of Herzberg-Teller and Born-Oppenheimer coupling," The Journal of Chemical Physics **4513**, 4513–4523 (1973).

[28]H. Köppel, W. Domcke, and L. S. Cederbaum, *Multimode Molecular Dynamics Beyond the Born-Oppenheimer Approximation*, edited by I. Prigogine and S. A. Rice, Vol. Advances in Chemical Physics, LVII (Wiley, 1984) pp. 59–246.

[29]W. Domcke, H. Köppel, and L. S. Cederbaum, "Spectroscopic effects of conical intersections of molecular potential energy surfaces," Molecular Physics **43**, 851–875 (1981).

[30]G. A. Worth, H. D. Meyer, and L. S. Cederbaum, "The effect of a model environment on the S2 absorption spectrum of pyrazine: A wave packet study treating all 24 vibrational modes," Journal of Chemical Physics **105**, 4412–4426 (1996).

[31]S. P. Neville, A. Stolow, and M. S. Schuurman, "Vacuum ultraviolet excited state dynamics of the smallest ring, cyclopropane. I. A reinterpretation of the electronic spectrum and the effect of intensity borrowing," Journal of Chemical Physics **149** (2018), 10.1063/1.5044392.

[32]D. R. Yarkony, "Nonadiabatic quantum chemistry-past, present, and future," Chemical Reviews **112**, 481–498 (2012).

[33]H. D. Meyer, U. Manthe, and L. S. Cederbaum, "The multiconfigurational time-dependent Hartree approach," Chemical Physics Letters **165**, 73–78 (1990).

[34]F. Gatti and G. A. Worth, *Multidimensional Quantum Dynamics: MCTDH Theory and Applications*, edited by H. D. Meyer (Wiley VCH, 2009).

[35]M. Yaghoubi Jouybari, Y. Liu, R. Improta, and F. Santoro, "Ultrafast dynamics of the two lowest bright excited states of cytosine and 1-methylcytosine: A quantum dynamical study," Journal of Chemical Theory and Computation **16**, 5792–5808 (2020), pMID: 32687360, https://doi.org/10.1021/acs.jctc.0c00455.

[36]D. Aranda and F. Santoro, "Vibronic spectra of pi-conjugated systems with a multitude of coupled states: A protocol based on linear vibronic coupling models and quantum dynamics tested on hexahelicene," Journal of Chemical Theory and Computation **17**, 1691–1700 (2021), pMID: 33606542, https://doi.org/10.1021/acs.jctc.1c00022.

[37]J. A. Green, M. Yaghoubi Jouybari, D. Aranda, R. Improta, and F. Santoro, "Nonadiabatic absorption spectra and ultrafast dynamics of dna and rna photoexcited nucleobases," Molecules **26**, 1743 (2021).

[38]H. Wang and M. Thoss, "Multilayer formulation of the multiconfiguration time-dependent Hartree theory," Journal of Chemical Physics **119**, 1289–1299 (2003).

[39]M. Schröter, S. D. Ivanov, J. Schulze, S. P. Polyutov, Y. Yan, T. Pullerits, and O. Kühn, "Exciton-vibrational coupling in the dynamics and spectroscopy of Frenkel excitons in molecular aggregates," Physics Reports **567**, 1–78 (2015).

[40]F. A. Schröder, D. H. Turban, A. J. Musser, N. D. Hine, and A. W. Chin, "Tensor network simulation of multi-environmental open quantum dynamics via machine learning and entanglement renormalisation," Nature Communications **10**, 1–10 (2019).

[41]J. Prior, A. W. Chin, S. F. Huelga, and M. B. Plenio, "Efficient simulation of strong system-environment interactions," Physical review letters **105**, 050404 (2010).

[42]A. W. Chin, Á. Rivas, S. F. Huelga, and M. B. Plenio, "Exact mapping between system-reservoir quantum models and semi-infinite discrete chains using orthogonal polynomials," Journal of Mathematical Physics **51** (2010), 10.1063/1.3490188, arXiv:1006.4507.

[43]A. Chin, J. Prior, R. Rosenbach, F. Caycedo-Soler, S. F. Huelga, and M. B. Plenio, "The role of non-equilibrium vibrational structures in electronic coherence and recoherence in pigment–protein complexes," Nature Physics **9**, 113–118 (2013).

[44]U. Schollwöck, "The density-matrix renormalization group in the age of matrix product states," Annals of physics **326**, 96–192 (2011).

[45]S. Mainali, F. Gatti, D. Iouchtchenko, P.-N. Roy, and H.-D. Meyer, "Comparison of the multi-layer multi-configuration time-dependent hartree (ml-mctdh) method and the density matrix renormalization group (dmrg) for ground state properties of linear rotor chains," The Journal of Chemical Physics **154**, 174106 (2021), https://doi.org/10.1063/5.0047090.

[46]C. Schnedermann, A. M. Alvertis, T. Wende, S. Lukman, J. Feng, F. A. Schröder, D. H. Turban, J. Wu, N. D. Hine, N. C. Greenham, *et al.*, "A molecular movie of ultrafast singlet fission," Nature communications **10**, 1–11 (2019).

[47]D. Tamascelli, A. Smirne, J. Lim, S. F. Huelga, and M. B. Plenio, "Efficient simulation of finite-temperature open quantum systems," Physical review letters **123**, 090402 (2019).

[48]A. J. Dunnett and A. W. Chin, "Matrix product state simulations of non-equilibrium steady states and transient heat flows in the two-bath spin-boson model at finite temperatures," Entropy **23**, 77 (2021).

[49]A. J. Dunnett and A. W. Chin, "Simulating quantum vibronic dynamics at finite temperatures with many body wave functions at 0 k," Frontiers in Chemistry **8**, 1195 (2021).

[50]O. V. Ovchinnikov, A. V. Evtukhova, T. S. Kondratenko, M. S. Smirnov, V. Y. Khokhlov, and O. V. Erina, "Manifestation of intermolecular interactions in FTIR spectra of methylene blue molecules," Vibrational Spectroscopy **86**, 181–189 (2016).

[51]D. Heger, J. Jirkovský, and P. Klán, "Aggregation of methylene blue in frozen aqueous solutions studied by absorption spectroscopy," Journal of Physical Chemistry A **109**, 6702–6709 (2005).

[52]G. A. Shahinyan, A. Y. Amirbekyan, and S. A. Markarian, "Photophysical properties of methylene blue in water and in aqueous solutions of dimethylsulfoxide," Spectrochimica Acta - Part A: Molecular and Biomolecular Spectroscopy **217**, 170–175 (2019).

[53]J. C. Dean, S. Rafiq, D. G. Oblinsky, E. Cassette, C. C. Jumper, and G. D. Scholes, "Broadband Transient Absorption and Two-Dimensional Electronic Spectroscopy of Methylene Blue," J. Phys. Chem. A **119**, 9098–9108 (2015).

[54]T. B. de Queiroz, E. R. de Figueroa, M. D. Coutinho-Neto, C. D. Maciel, E. Tapavicza, Z. Hashemi, and L. Leppert, "First principles theoretical spectroscopy of methylene blue: Between limitations of time-dependent density functional theory approximations and its realistic description in the solvent," The Journal of Chemical Physics **154**, 044106 (2021), https://doi.org/10.1063/5.0029727.

[55]M. G. Mavros, D. Hait, and T. Van Voorhis, "Condensed phase electron transfer beyond the condon approximation," The Journal of Chemical Physics **145**, 214105 (2016).

[56]T. J. Zuehlsdorff, A. Montoya-Castillo, J. A. Napoli, T. E. Markland, and C. M. Isborn, "Optical spectra in the condensed phase: Capturing anharmonic and vibronic features using dynamic and static approaches," J. Chem. Phys **151**, 074111 (2019).

[57]S. Mukamel, *Principles of Nonlinear Optical Spectroscopy* (Oxford University Press, New York, 1995).

[58]M. Cho, "Coherent two-dimensional optical spectroscopy," Chem. Rev. **108**, 1331–1418 (2008).

[59]F. Duschinsky, "," Acta Physicochim. URSS. **7**, 411 (1937).

[60]J. S. Bader and B. J. Berne, "Quantum and classical relaxation rates from classical simulations," J. Chem. Phys. **100**, 8359 (1994).

[61]S. A. Egorov, K. F. Everitt, and J. L. Skinner, "Quantum Dynamics and Vibrational Relaxation," J. Phys. Chem. A **103**, 9494–9499 (1999).

[62]H. Kim and P. J. Rossky, "Evaluation of Quantum Correlation Functions from Classical Data," J. Phys. Chem. B **106**, 8240

(2002).
[63]S. Valleau, A. Eisfeld, and A. Aspuru-Guzik, "On the alternatives for bath correlators and spectral densities from mixed quantum-classical simulations," J. Chem. Phys. **137**, 224103 (2012).
[64]I. R. Craig and D. E. Manolopoulos, "Quantum statistics and classical mechanics: Real time correlation functions from ring polymer molecular dynamics," J. Chem. Phys. **121**, 3368 (2004).
[65]R. Ramirez, T. Lopez-Ciudad, P. K. P, and D. Marx, "Quantum corrections to classical time-correlation functions: Hydrogen bonding and anharmonic floppy modes," J. Chem. Phys. **121**, 3973 (2004).
[66]T. Pacher, L. S. Cederbaum, and H. Köppel, "Approximately diabatic states from block diagonalization of the electronic hamiltonian," The Journal of Chemical Physics **89**, 7367–7381 (1988), https://doi.org/10.1063/1.455268.
[67]J. E. Subotnik, S. Yeganeh, R. J. Cave, and M. A. Ratner, "Constructing diabatic states from adiabatic states: Extending generalized mulliken–hush to multiple charge centers with boys localization," The Journal of Chemical Physics **129**, 244101 (2008), https://doi.org/10.1063/1.3042233.
[68]T. Van Voorhis, T. Kowalczyk, B. Kaduk, L.-P. Wang, C.-L. Cheng, and Q. Wu, "The diabatic picture of electron transfer, reaction barriers, and molecular dynamics," Annual Review of Physical Chemistry **61**, 149–170 (2010), pMID: 20055670, https://doi.org/10.1146/annurev.physchem.012809.103324.
[69]C. E. Hoyer, X. Xu, D. Ma, L. Gagliardi, and D. G. Truhlar, "Diabatization based on the dipole and quadrupole: The dq method," The Journal of Chemical Physics **141**, 114104 (2014), https://doi.org/10.1063/1.4894472.
[70]G. R. Medders, E. C. Alguire, A. Jain, and J. E. Subotnik, "Ultrafast electronic relaxation through a conical intersection: Nonadiabatic dynamics disentangled through an oscillator strength-based diabatization framework," The Journal of Physical Chemistry A **121**, 1425–1434 (2017).
[71]M. F. Gelin and R. Borrelli, "Simulation of nonlinear femtosecond signals at finite temperature via a thermo field dynamics-tensor train method: General theory and application to time- and frequency-resolved fluorescence of the fenna–matthews–olson complex," Journal of Chemical Theory and Computation (2021).
[72]T. J. Zuehlsdorff, H. Hong, L. Shi, and C. M. Isborn, "Nonlinear spectroscopy in the condensed phase: The role of duschinsky rotations and third order cumulant contributions," The Journal of Chemical Physics **153**, 044127 (2020).
[73]P. Eastman, J. Swails, J. D. Chodera, R. T. McGibbon, Y. Zhao, K. A. Beauchamp, L.-P. Wang, A. C. Simmonett, M. P. Harrigan, C. D. Stern, R. P. Wiewiora, B. R. Brooks, and V. S. Pande, "Openmm 7: Rapid development of high performance algorithms for molecular dynamics," PLOS Comput. Biol. **13**, 1–17 (2017).
[74]W. L. Jorgensen, J. Chandrasekhar, and J. D. Madura, "Comparison of simple potential functions for simulating liquid water," J. Chem. Phys. **79**, 926 (1983).
[75]J. T. Horton, A. E. A. Allen, L. S. Dodda, and D. J. Cole, "Qubekit: Automating the derivation of force field parameters from quantum mechanics," J. Chem. Inf. Model **59**, 1366–1381 (2019).
[76]I. S. Ufimtsev and T. J. Martinez, "Quantum Chemistry on Graphical Processing Units. 3. Analytical Energy Gradients and First Principles Molecular Dynamics," J. Chem. Theory Comput. **5**, 2619–2628 (2009).
[77]T. Yanai, D. P. Tew, and N. C. Handy, "A new hybrid exchange-correlation functional using the Coulomb-attenuating method (CAM-B3LYP)," Chem. Phys. Lett. **393**, 51–57 (2004).
[78]C. M. Isborn, N. Luehr, I. S. Ufimtsev, and T. J. Martínez, "Excited-State Electronic Structure with Configuration Interaction Singles and Tamm–Dancoff Time-Dependent Density Fucntional Theory on Graphical Processing Units," J. Chem. Theory Comput. **7**, 1814–1823 (2011).
[79]P. J. Stephen, F. J. Devlin, C. F. Chabalowski, and M. J. Frisch, "Ab Initio Calculation of Vibrational Absorption," The Journal of Physical Chemistry **98**, 11623–11627 (1994).
[80]M. C. Zwier, J. M. Shorb, and B. P. Krueger, "Hybrid Molecular Dynamics-Quantum Mechanics Simulations of Solute Spectral Properties in the Condensed Phase: Evaluation of Simulation Parameters," J. Comput. Chem. **28**, 1572–1581 (2007).
[81]A. M. Rosnik and C. Curutchet, "Theoretical Characterization of the Spectral Density of the Water-Soluble Chlorophyll-Binding Protein from Combined Quantum Mechanics/Molecular Mechanics Molecular Dynamics Simulations," J. Chem. Theory Comput. **11**, 5826–5837 (2015).
[82]S. Chandrasekaran, M. Aghtar, S. Valleau, A. Aspuru-Guzik, and U. Kleinekathöfer, "Influence of Force Fields and Qauntum Chemistry Approach on Spectral Densities of BChl *a* in Solution and in FMO Proteins," J. Phys. Chem. B **119**, 9995–10004 (2015).
[83]C. W. Kim, J. W. Park, and Y. M. Rhee, "Effect of Chromophore Potential Model on the Description of Exciton–Phonon Interactions," J. Phys. Chem. Lett. **6**, 2875–2880 (2015).
[84]M. K. Lee and D. F. Coker, "Modeling Electronic-Nuclear Interactions for Excitation Energy Transfer Processes in Light-Harvesting Complexes," J. Phys. Chem. Lett. **7**, 3171–3178 (2016).
[85]O. Andreussi, I. G. Prandi, M. Canpetella, G. Prampolini, and B. Mennucci, "Classical Force Fields Tailored for QM applications: Is it Really a Feasible Strategy?" J. Chem. Theory Comput. **13**, 4636–4648 (2017).
[86]T. J. Zuehlsdorff, "Molspeckpy: Spectroscopy python code, available on github: https://github.com/tjz21/spectroscopy_python_code," (2021).
[87]J. Haegeman, C. Lubich, I. Oseledets, B. Vandereycken, and F. Verstraete, "Unifying time evolution and optimization with matrix product states," Phys. Rev. B **94**, 165116 (2016).
[88]B. Kloss, Y. B. Lev, and D. Reichman, "Time-dependent variational principle in matrix-product state manifolds: Pitfalls and potential," Physical Review B **97**, 024307 (2018).
[89]M. Woods, M. Cramer, and M. Plenio, "Simulating Bosonic Baths with Error Bars," Physical Review Letters **115**, 130401 (2015).
[90]A. Fernández-Pérez, T. Valdés-Solís, and G. Marbán, "Visible light spectroscopic analysis of methylene blue in water; the resonance virtual equilibrium hypothesis," Dyes and Pigments **161**, 448–456 (2019).
[91]F. J. Avila Ferrer and F. Santoro, "Comparison of vertical and adiabatic harmonic approaches for the calculation of the vibrational structure of electronic spectra," Phys. Chem. Chem. Phys. **14**, 13549–13563 (2012).